PHYSICAL REVIEW B VOLUME 51, NUMBER 24 15 JUNE 1995-II

Atomic and electronic structure of icosahedral Al-Pd-Mn alloys and approximant phases

M. Krajčí,* M. Windisch, J. Hafner, and G. Kresse
Institut für Theoretische Physik, Technische Universität Wien, Wiedner Hauptstraße 8-10/136, A-1040 Wien, Austria

M. Mihalkovič
Institute of Physics, Slovak Academy of Sciences, Dúbravská cesta 9, SK 84228 Bratislava, Slovakia
(Received 30 January 1995)

The electronic structures of the stable face-centered-icosahedral alloy $Al_{70}Pd_{20}Mn_{10}$ and of a hierarchy of rational approximants to the icosahedral phase have been calculated using *ab initio* pseudopotential, linear-muffin-tin-orbital (LMTO), and tight-binding (TB)-LMTO techniques. The description of the atomic structure is based on a projection from six-dimensional space, with acceptance volumes chosen such as to reproduce the observed diffraction data. For the lowest-order approximants (1/1 and 2/1 with 128 and 544 atoms in the periodically repeated cell), the electronic eigenvalues and eigenfunctions have been calculated self-consistently using LMTO and *ab initio* pseudopotential techniques. For the 1/1 approximant, we have also performed a relaxation of the idealized structure using the Hellmann-Feynman forces. For the higher-order approximants (we go up to the 8/5 approximants with 41 068 atoms), the electronic densities of states and the spectral functions have been calculated from the TB-LMTO Hamiltonian via a real-space recursion technique. The electronic density of states (DOS) of the higher-order approximants is characterized by a structure-induced minimum at the Fermi level, indicating the possibility of a Hume-Rothery-type electronic mechanism for the stabilization of the icosahedral phase. However, in the lowest-order approximants the DOS minimum is either flattened or shifted away from the Fermi energy. This is in contrast to the simple icosahedral alloys such as Al-Cu-Li, where the DOS minimum exists in the quasiperiodic phase and in the crystalline approximants. Hence it appears that for the face-centered icosahedral alloys, the structure-induced DOS minimum may be not only a generic, but also a specific property of the quasicrystalline phase. In addition to the spectral properties, we have also studied the character of the electronic states via a calculation of the participation ratio. We find that the states in the vicinity of the Fermi level tend to be more localized than in the rest of the valence band and that the localization is related to certain aspects of the quasicrystalline structure. This is important for understanding the anomalous transport properties of these alloys.

I. INTRODUCTION

Ever since the discovery of an icosahedral phase in the Al-Mn system,[1] the question whether the quasiperiodic order leads to specific physical properties different from those of the crystalline or amorphous phases has been a subject of intense debate.[2–4] The first quasicrystals were thermodynamically metastable, their diffraction patterns exhibited significant structural disorder so that it was difficult to detect physical properties intrinsic to the quasiperiodic state. There have been early suggestions,[5–7] based largely on electron-counting arguments, that the energetic stability of the quasicrystalline phases is promoted by a Hume-Rothery-like mechanism, leading to the formation of a structure-induced pseudogap in the electronic density of states (DOS) at the Fermi level. Indeed the investigation of the electronic properties of such quasicrystals (both experimentally[3,4] and theoretically[8–11]) has demonstrated that the structure-induced pseudogap is a *generic* property of the quasicrystalline alloys. However, it was also demonstrated that it is not a *specific* property–structure-induced pseudogaps exist also in the crystalline and amorphous phases of similar composition.[10]

The discovery[12,13] of thermodynamically stable icosahedral alloys in the Al-Cu-M (M = Fe, Ru, Os) and Al-Pd-M (M = Mn, Re) systems—with a high structural perfection was therefore an important step towards an answer to that fundamental question. Indeed these alloys show very unusual physical properties, such as very high electrical resistivities (up to 0.03 Ω cm in Al-Cu-Ru alloys[3] and up to 0.28 Ω cm in Al-Pd-Re alloys[14]) increasing with structural perfection of the samples,[15] strong negative temperature coefficients of the resistivity, and low density of states at the Fermi level. These properties place the stable icosahedral alloys close to a metal-insulator transition. Because of their striking characteristics, the stable icosahedral alloys are the most attractive testing ground for theories of the electronic properties of quasicrystalline alloys. However, there are two main obstacles to the formulation of such a theory. (i) A prerequisite to a calculation of the electronic spectrum is that the atomic structure is well known even in its details, but structural models for the stable icosahedral

0163-1829/95/51(24)/17355(24)/$06.00

phases are still a subject of debate.[16] (ii) With a few exceptions[10,11] most calculations of the electronic properties of icosahedral alloys are based on structural models for the lowest-order approximants.[8,9,17] This may be a justifiable approximation for most of the metastable icosahedral alloys such as *i*-Al-Cu-Li where there are only minimal differences in the electronic densities of states and small differences in the electric transport properties of the quasiperiodic phases and their 1/1 approximants (the *R*-phase of Al-Cu-Li in this case).[11,18] For the stable icosahedral phases, no stable 1/1 approximants are known (we should differentiate between the rational approximants constructed by projection from higher dimensional space, and crystalline phases that merely show some similarity in the short-range order with the quasicrystalline phases). This may even be an important hint as to the reasons for the high structural perfection of these phases, as it demonstrates that the energetic cost for the creation of phason defects is very high. Hence, one has to solve the problems of an accurate structural modeling and of the calculation of the electronic spectrum for models that are sufficiently large to allow one to extrapolate to the quasiperiodic limit.

The recently discovered stable icosahedral Al-Pd-Mn phase[19] has been selected as the most promising candidate for such a study. These alloys are completely free of atomic disorder and phason strains even if produced by rapid solidification.[20] The atomic structure has been studied by x-ray and neutron diffraction (including contrast-variation techniques),[16,21–26] extended x-ray absorption fine-structure (EXAFS) measurements,[27] and various techniques based on electron microscopy.[28] The analysis of the diffraction data has led to first-order models of the atomic structure,[24,29] based on spherical atomic surfaces in the perpendicular subspace $E_\perp$ of the six-dimensional (6D) space. This model has later been refined by Katz and Gratias[30] and by Cockayne *et al.*,[31] by introducing triacontahedral atomic surfaces. The very high electrical resistivities[32,33] (up to 10 000 $\mu\Omega$ cm, depending critically on sample preparation and composition) have been taken as evidence for a low density of states at the Fermi level, and this is confirmed by measurements of the electronic specific heat.[34] The temperature and magnetic-field dependence of the electrical resistivity have been interpreted within the framework of theories of weak localization.[32,33,35] All these results corroborate the picture of a material close to a metal/insulator transition. However, direct experimental evidence for the existence of a pseudogap around the Fermi level should also be based on information on the DOS below and above E_F. The DOS of the occupied part of the valence band of *i*-Al-Pd-Mn has been investigated using x-ray and ultraviolet photoemission spectroscopy (Refs. 36 and 37) and soft-x-ray emission spectroscopy (SXE) (Ref. 38); the DOS of the empty states has been probed via soft-x-ray absorption spectroscopy (SXA).[38] However, a critical analysis of the potential of state-of-the-art spectroscopies[39] has emphasized that it is very hard to present conclusive spectroscopic evidence for the existence of narrow pseudogaps.

In the present work, we concentrate on the theoretical prediction of the electronic spectrum of icosahedral Al-Pd-Mn. Our description of the atomic structure is based on the projection model with triacontahedral atomic surfaces proposed by Katz and Gratias[30] and Cockayne *et al.*,[31] refined such as to produce the proper chemical short-range order and the correct interatomic distances. We show that for the larger approximants, good agreement with even the details of the measured neutron-diffraction data can be achieved. The projection method can also be used to determine the lower-order approximants (for the 2/1 approximant see Waseda *et al.*[40]), but for the 1/1 approximant, it turns out that the projection results either in a chemical composition or in a local order rather different from the icosahedral phase. The electronic spectrum of the entire hierarchy of approximants ranging from the 1/1 phase with 128 atoms in the cell up to the 8/5 approximants with 41 068 atoms has been calculated using the linear-muffin-tin-orbital (LMTO),[41] pseudopotential-based *ab initio* molecular-dynamics (MD) (Refs. 42 and 43), and tight-binding–linear-muffin-tin-orbital (TB-LMTO) (Refs. 44 and 45) techniques. For the 1/1 and 2/1 approximants, we can calculate the eigenvalues and eigenstates of the electrons by direct diagonalization of the Hamiltonian; for the higher-order approximants, we can calculate only the total, local, and angular-momentum projected densities of state and the total and partial Bloch-spectral functions. The *ab initio* MD technique also allows us to test the stability of the lowest-order approximants by relaxing the ideal structure using the exact Hellmann-Feynman forces.

The comparison with the measured photoelectron and soft-x-ray spectra shows that our calculated electronic structure is very realistic. The important result of this study, however, is to demonstrate the existence of a hierarchy of structure-induced gaps at each level of approximation to the quasiperiodic limit. Only close to this limit do these gaps interfere to form a pseudogap that is sufficiently close to the Fermi level and sufficiently wide to make a significant contribution towards an energetic stabilization of the quasicrystalline phase. In the low-order approximants (in particular, in the different versions of the 1/1 approximants) the pseudogap splits into several smaller gaps at a certain distance from E_F, so that these phases receive less or no electronic stabilization. This is the only known example where the electronic-structure calculation reveals a significant difference between the electronic structures of a quasiperiodic alloy and its approximants.

In addition, we have examined the localization properties of the electronic eigenstates in the entire valence band. We find that the states in the vicinity of the Fermi level tend to be more localized than states far from the pseudogap. Hence, the anomalous electric transport properties are due not only to the low DOS (resulting in a reduction of the number of carriers), but in addition to a reduced mobility of the electrons in states contributing to the transport properties. We also find a striking correlation between localization and quasicrystallinity: The amplitude of the localized states close to the Fermi level (these are mostly Mn states) is largest on those atomic

sites with the shortest vectors in perpendicular space. This is at least a step towards an understanding of the structural origin of the transport anomalies.

II. STRUCTURAL MODELING

Previous structural work on icosahedral Al-Pd-Mn is based on neutron-diffraction investigations with isomorphous substitution of the Mn-atoms by a Fe-Cr mixture[22] and on the simultaneous analysis of the neutron-diffraction and x-ray diffraction data (including anomalous x-ray diffraction).[24–26] This has led to a model for the atomic structure, based on the projection of a face-centered hypercubic lattice in 6D onto the 3D physical space $E_{\|}$, resulting in a face-centered (or F-type) icosahedral lattice. In a first approximation, the atomic surfaces in the perpendicular subspace $E_{\perp}$ of the 6D space E_6 are described by spheres and spherical shells. These shells are located at the lattice points of the 6D face-centered hypercubic lattice, described as a superstructure of the 6D simple hypercubic lattice. For i-Al-Pd-Mn, one needs six different atomic surfaces: a Mn core and outer Al shell at the "even" nodes ($n_0 = [000\,000]$), a Mn core surrounded by an inner Pd shell, and an outer Al shell at the "odd" nodes ($n_1 = [100\,000]$), and a Pd sphere at the bc_0 positions ($bc_0 = \frac{1}{2}[111\,111]$) (see Fig. 1). The inequivalence of the atomic surfaces centered at the even and odd nodes breaks the simple cubic symmetry of the 6D lattice and leads to a face-centered superstructure. This modeling based on the three different atomic surfaces has first been proposed by Cornier-Quinandon *et al.*[29] for i-Al-Cu-Fe, the division into subshells accounts for the chemical order in the system. In our work, we have adopted the triacontahedral atomic surfaces proposed by Katz and Gratias[30] and by Cockayne *et al.*[31] A triacontahedron with a fivefold radius τ^2 (in units of the edge of the rhombohedra of the underlaying Penrose lattice) at n_0; an identical triacontahedron at n_1, except truncated by its intersections with its 12 images displaced by τ^3 along the fivefold axes; and a triacontahedron with radius 1 at bc_0. The division into subshells is analogous to the spherical model, with radii in the ratio $2\tau^{-1} : 2 : \tau^2$ for the shells centered at n_1 and $1 : \tau^2$ for those centered at n_0. The model is illustrated in Fig. 1 through cross sections of the atomic surfaces in perpendicular space.

A. Rational approximants

For the construction of periodic or rational approximants to the quasicrystalline lattice, the perpendicular space is deformed in such a way that in the icosahedral basis vectors in $E_{\perp}$ [$\mathbf{e}'_l = C(1, -\tau, 0)$ + cyclic permutations (c.p.) for $l = 1, 2, 3$, and $\mathbf{e}'_l = C(1, \tau, 0)$ + c.p. for $l = 4, 5, 6$ where C is a constant normalizing the basis vectors to unity] the Golden mean τ is replaced by a rational approximant $\tau_n = F_{n+1}/F_n$, where the F_n are Fibonacci numbers defined by the recursion sequence $F_{n+1} = F_n + F_{n-1}$; $F_1 = F_2 = 1$. For an approximant, the position of the acceptance domain in $E_{\perp}$ is not

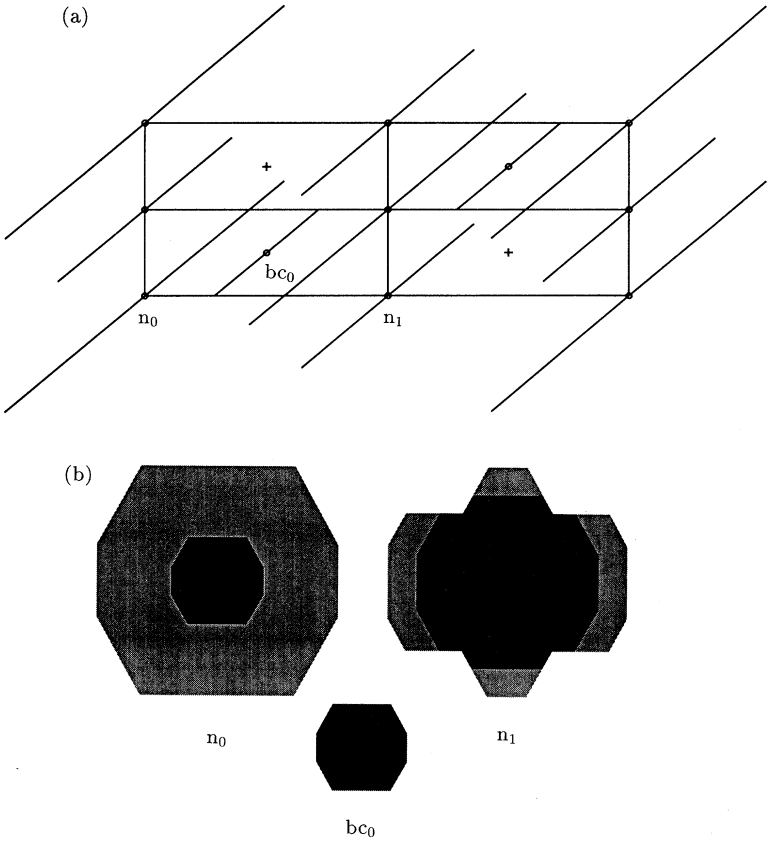

FIG. 1. Illustration of our model for the structure of icosahedral Al-Pd-Mn. (a) Section through the 6D space containing the fivefold axes in $E_{\|}$ and $E_{\perp}$. Atomic surfaces are placed at the nodes n_i and the body centers bc_0 of a hypercubic lattice. Since the atomic surfaces placed on the even and odd nodes (n_0 and n_1) are not equivalent, the symmetry of the 6D lattice is face-centered cubic. (b) Cross sections through the atomic surfaces (calculated for a 13/8 approximant). The Mn cores at the n_0 and n_1 nodes are represented by the darkest shading; the lighter shading represents the outer Pd and Al shells at these nodes and the Pd surface at the bc_0 position.

fixed. For each approximant there exists a periodically repeated zone Z of nonequivalent shifts of the atomic surfaces in $E_\perp$. The edge of this cubic zone has the length $z = 1/\sqrt{F_{n+1}^2 + F_n^2}$, the zone shrinks to a point in the quasiperiodic limit. The shift $\mathbf{t}_s = \frac{1}{2}(1,1,1)z$ places the center of the acceptance domain on the body-centered position of the zone Z and defines a special class of symmetrical models. A shift $\mathbf{t}_s \neq (0,0,0)$ avoids singularities arising from points that lie exactly on the boundary of the acceptance domain.

If a simple hypercubic lattice is projected onto the 3D space, the structure of the approximant is body-centered cubic for $\mathrm{mod}(n,3) = 1$ and simple cubic otherwise. The face-centered superstructure of the 6D quasilattice of the F-type icosahedral quasicrystals leads to a change in the Bravais class, so that all approximants are simple cubic with the symmetry group $P2_13$. The rational approximation also leads to a deformation of the atomic surfaces and hence to a change in stoichiometry. The acceptance domains for the lower-order approximants were constructed as the Voronoi polyhedra to vectors constraining the short interatomic distances in the model. The standard model (referred to as model $1/1 - M2$ in the following) for the lowest-order (1/1) approximant contains 15.6 at. % Mn compared to the 8.6 at. % of the icosahedral phase. To construct a 1/1 approximant with a composition closer to that of the quasicrystal, the inner Mn atomic surface at the even nodes was reduced from $2\tau^{-1}$ to 1. This leads to a Mn concentration of 6.2 at. %, but also to less realistic interatomic distances. The number of atoms and compositions of all rational approximants considered in this study are given in Table I.

In the Al-Pd-Mn system, an as-quenched icosahedral $Al_{70}Pd_{26}Mn_4$ alloy transforms into a 2/1 cubic crystalline approximant at 1023 K (Ref. 40). The 2/1 approximant with the smaller Mn atomic surfaces (2/1-$M1$) is rather close to the chemical composition of this phase so that the structures produced by our model can be tested against experiment at least at this level.

B. Comparison with experiment: Total and partial structure factors

Figure 2 shows the neutron powder-diffraction pattern, as calculated for the largest model (the 8/5 approximant with 41 068 atoms in the periodically repeated cell), compared to the experimental data of Boudard *et al.*[24] Figure 3 shows a comparison of the most intense Bragg reflections for x-ray scattering from single-crystal samples. This demonstrates that the model is in good overall agreement with experiment.

Because of the evident importance of chemical ordering in describing the structure of *i*-Al-Pd-Mn, attempts have been made to determine partial structure factors by contrast variation in neutron scattering ("isomorphic" substitution of Mn by a Fe-Cr alloy)[22] and in x-ray scattering (anomalous diffraction on the Pd edge).[46] The neutron-diffraction experiment yields partial structure factors F_{AlPd} and F_T, T=Mn(FeCr), the anomalous x-ray diffraction experiment and the partial structure factor F_{Pd}. Figures 4 and 5 show the dependence of the partial structure factors on the wave vector $|\vec{Q}_p|$ in perpendicular reciprocal space $E_\perp^\star$. The partial structure factors may be decomposed in two classes: (i) In the indexing scheme proposed by Cahn *et al.*[47] (see also Fig. 2), the indices N and M have the same parity, and (ii) N and M have opposite parity. Within each class, one may distiguish between primitive (P) reflections (N even) and superstructure (S) reflections (N odd). Figure 4 shows the partial Pd-structure factor determined by the anomalous x-ray diffraction experiment and as calculated by the spherical model of Cornier-Quinandon *et al.*[29] and using the atomic surfaces defined above. Both models reproduce the measured structure factor rather well, the facetting of the atomic surfaces turns out to have only little influence on the partial structure factor. The most significant difference between theory and experiment is the more rapid decay of the experimental structure factor at large values of $Q_\perp$. This difference has been discussed by de Boissieu *et al.*[16,26,46] in terms of the geometry of the atomic surfaces and of bounded fluctuations of the atomic surfaces in perpendicular space. These fluctua-

TABLE I. Number of atoms N_{atom} and chemical composition (in at. %) of the rational approximants to icosahedral Al-Pd-Mn.

Approximant	N_{atom}	c_{Al}	c_{Pd}	c_{Mn}
1/1 ($M1$)	128	68.8	25.0	6.2
1/1 ($M2$)	128	68.8	15.6	15.6
2/1 ($M1$)	544	68.4	25.7	5.9
2/1 ($M2$)	544	68.4	22.8	8.8
3/2	2292	70.3	20.6	9.1
5/3	9700	70.6	20.7	8.7
8/5	41068	70.8	20.6	8.6
13/8	173936	70.8	20.6	8.6

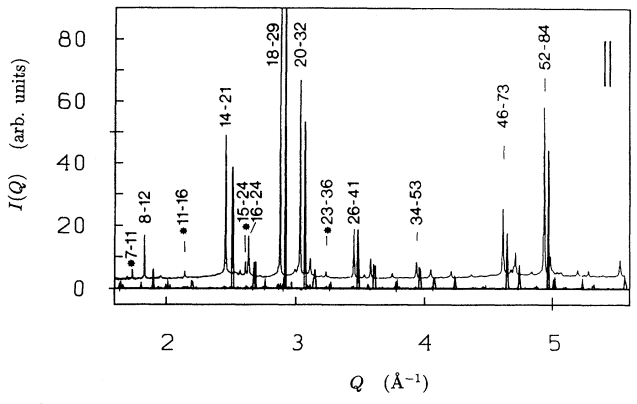

FIG. 2. Comparison of the neutron powder-diffraction pattern calculated for the 8/5 approximant to icosahedral Al-Pd-Mn with the high-resolution data of Boudard *et al.* (Ref. 24). The main Bragg reflections are indexed according to the scheme proposed by Cahn *et al.* (Ref. 47). For the sake of clarity, the experimental diffraction pattern has been shifted to the left by a constant amount (indicated by the vertical bars in the upper right corner).

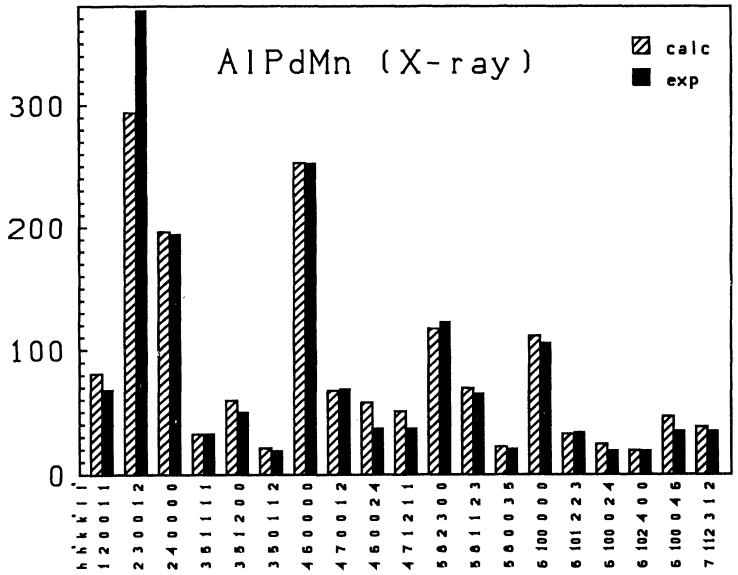

FIG. 3. Comparison of the most intense x-ray single-crystal diffraction peaks as calculated for the 8/5 approximant to icosahedral Al-Pd-Mn, with the experimental data of Boudard *et al.* (Ref. 24). The Bragg peaks are indexed in a 6D notation.

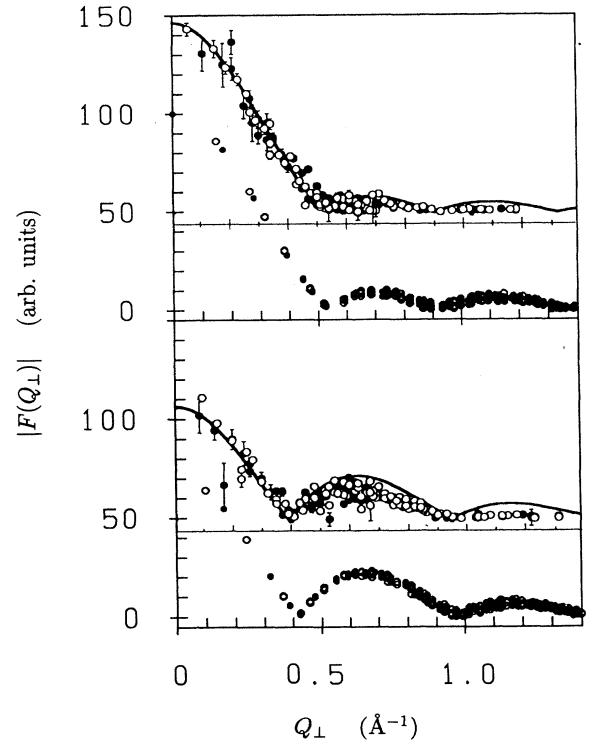

FIG. 4. Comparison of the calculated partial structure factor $F_{\mathrm{Pd}}(Q_\perp)$ for *i*-Al-Pd-Mn, with the anomalous x-ray diffraction data of Ref. 46. The upper part of the figure represents the results for reflections with N and M (in the notation of Cahn *et al.*[47]) with the same parity, the lower part corresponds to reflections with N and M having different parity. In both cases, the full (open) circles are the $P(S)$ reflections having N even (odd). The data with error bars refer to the experiment, the data calculated for our model have been shifted for sake of clarity. The full lines represent the spherical model of Cornier-Quinandon *et al.*[29] Cf. text.

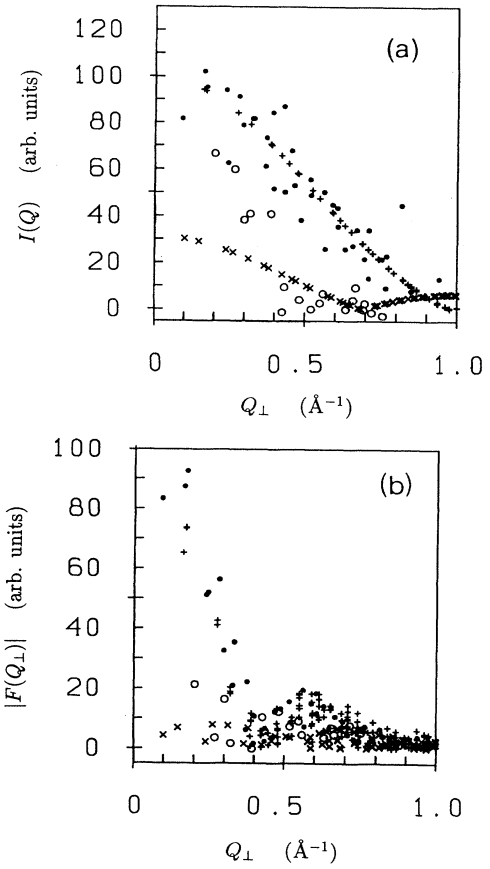

FIG. 5. Comparison of the calculated partial structure factors $F_{\mathrm{AlPd}}(Q_\perp)$ (a) and $F_T(Q_\perp)$, T=Mn(FeCr) (b), for *i*-Al-Pd-Mn with the result of the neutron-diffraction experiment with isomorphic substitution (Ref. 22). The full and open circles represent the experimental results for reflections with N and M having the same parity and N and M of different parity, respectively. + and × represent the theoretical results corresponding to the full and empty circles. See text.

tions lead to a random phason disorder that does not affect the long-range order determining the Bragg peaks, but leads to a damping of their intensities by a phason Debye-Waller term. The comparison of our model with the spherical model suggests that difference between model and experiments has to be attributed mainly to the phason fluctuations. Here, we shall not pursue this difference any further, because it is not possible at the moment to study the influence of phason disorder on the electronic structure but we note that, apart from possible phason fluctuations, the structural model is quite realistic. Figure 5 shows the corresponding results for the AlPd and T structure factors. The lower accuracy of the isomorphic substitution experiment is reflected by the large scatter of the experimental data, but within these limits the agreement is again satisfactory.

The local chemical order and topology is also probed by an EXAFS experiment. Table II compares the nearest-neighbor coordination numbers and distances calculated for the 5/3 approximant with the experimental data of Sadoc and Dubois[27,48] for the i phase. All atom pairs for distances up to 3 Å have been listed. Considering that the EXAFS experiment is not always able to resolve subshells, we find a very encouraging agreement between theory and experiment. In particular, the experiment confirms the surprisingly low coordination numbers resulting from the six-dimensional model.

The x-ray powder-diffraction pattern for the 2/1 approximant has been measured by Waseda *et al.*[40] Figure 6 demonstrates good agreement between theory (approximant 2/1 $M1$) and experiment. This is important since it shows that the modification of the inner Mn shell leads to realistic structures for the low-order approximants.

TABLE II. First coordination shells around Al, Pd, and Mn atoms in i-Al-Pd-Mn: N_c coordination number, d interatomic distance, and σ width of the nearest-neighbor shell estimated from the EXAFS data. The theoretical results refer to the 5/3 approximant; the experimental data are taken from Sadoc and Dubois (Refs. 27, 48).

Central atom	Neighbor atom	Theory N_c	Theory ΣN_c	Theory d (Å)	Expt. N_c	Expt. d (Å)	Expt. σ (Å)
Al	Al	2.61		2.57			
		5.27	7.88	2.96	7.0	2.80	0.20
	Pd	1.65		2.57	1.5	2.60	0.18
		0.50	2.15	2.82			
		0.65	2.80	2.96			
	Mn	0.81		2.57	1.0	2.50	0.20
		0.45	1.26	2.96			
Pd	Al	5.63		2.57	5.8	2.60	0.09
		1.69	7.32	2.82			
		2.21	9.53	2.96			
	Pd	2.24		2.96	2.2	3.10	0.11
	Mn	0.12		2.57			
		0.02	0.14	2.82	0.5	2.75	0.12
		0.01	0.15	2.96			
Mn	Al	6.57		2.57	7.0	2.50	0.11
		3.61	9.18	2.96			
	Pd	0.29		2.57			
		0.06	0.35	2.82	1.0	2.75	0.11
		0.03	0.38	2.96			

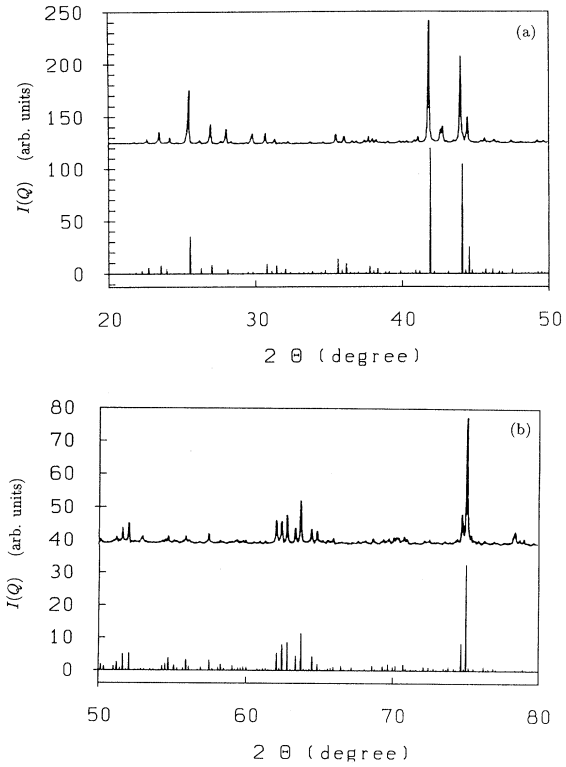

FIG. 6. (a,b) Calculated x-ray powder-diffraction pattern (lower curves) for the 2/1-approximant $Al_{68.4}Pd_{25.7}Mn_{5.9}$, compared with the experimental data (upper curves) of Waseda *et al.* (Ref. 40) for the as-quenched 2/1-phase $Al_{70}Pd_{26}Mn_4$.

C. Atomic-shell structure of the quasicrystalline phase

The description of the icosahedral structures in terms of a dense packing of large icosahedral clusters has been invoked for the interpretation of some of their striking physical properties. The relatively low coordination numbers calculated for our model (and confirmed by the EXAFS experiments) seem to be hard to reconcile with such a picture. We have, therefore, performed a detailed analysis of the coordination shells. For the 1/1 approximant, we find 14 inequivalent crystallographic sites. For most of these sites, the inner coordination shells have only a very low symmetry [for the space group $P2_13$ there are only two classes of atomic positions: 12(b) with no point symmetry, and 4(a) with point symmetry 3], with the exception of the Pd atom in the bc_0 position with an icosahedron as the first and a pentagonal dodecahedron as the second coordination shell. The shells for the 14 inequivalent positions are shown in Fig. 7. Sites 1 to 3 are occupied by Mn atoms. The irregular first coordination shells consist of seven to nine Al atoms and a small number of Pd and Mn atoms. It is followed by a regular icosahedron of Pd and Mn atoms around site 1 and 10 Al and 2 Mn atoms around sites 2 and 3. Sites 4 to 6 are occupied by Pd atoms. Site 4 is projected from the center of the atomic surface at the body-centered position at bc_0, it

therefore has an atomic environment with full icosahedral symmetry in the quasiperiodic limit, and nearly complete icosahedral symmetry in the approximants. Sites 5 and 6 have again a low-symmetry environment. Sites 7 to 14 are occupied by Al atoms with a seemingly completely irregular coordination. It is worthwhile to point out that the irregular coordination polyhedra result from a truncation of shells with full icosahedral symmetry (details see below). This is seen most easily at the example of the third shells at sites 7, 8, 9, and 12, where one recognizes fragments of a regular icosahedron. The symmetry of the local environments is important for understanding the variations in the local DOS, see Sec. IV.

For the higher-order approximants, we find that shells of lower symmetry alternate with highly symmetric shells. As two examples, we show in Figs. 8(a) and 8(b) the first ten coordination shells around one of the seven fold coordinated Mn sites (this site is projected from the point closest to the center of the Mn-acceptance domain centered at the even nodes n_0) and around the highly symmetric icosahedral Pd site (projected from the bc_0 center) in the 5/3 approximant. To emphasize the site symmetry, the successive shells are shown looking down along the fivefold and twofold symmmetry axes. Around the Mn sites [see Fig. 8(a)], the innermost shell consisting of seven atoms only is surrounded by 12- and 30-atom shells with perfect icosahedral symmetry, but then follow incomplete shells with 36 and again 7 atoms. This seven-atom shell is a τ^2 scaled version of the innermost shell. Next, follow an irregular 24-atom shell and icosahedral shells with 30 (a scaled version of the third shell), 60, and 72 atoms, while the tenth shell with 30 atoms is a distorted icosahedral configuration. Around the "symmetric" Pd site [Fig. 8(b)] the two innermost icosahedral shells with 12 and 20 atomic sites (a regular icosahedron and a pentagonal dodecahedron) are followed by two distorted shells, with 24 atoms each and again icosahedral shells with 20 and 12 atoms. From the point of view of the topology, these shells are exactly τ-, respectively, τ^2-scaled versions of the inner shell, but they differ in the chemical occupancy (which breaks the overall symmetry). Note that what looks like a random distribution of the chemical species is in fact an ordered arrangement determined by the projection from 6D space. Farther out follow shells with perfect icosahedral symmetry (but again mixed chemical occupancy), until in the 17th shell a 24-atom cluster with distorted icosahedral symmetry appears (not shown).

The comparsion with the 1/1 approximant (site 4 in Fig. 7) shows that for this site with local icosahedral symmetry, the rational approximation changes the local chemical order: the dodecahedral shell is occupied in the higher-order approximant (and in the icosahedral phase) by Pd atoms only, whereas it has mixed Al-Pd-Mn occupancy in the low-order approximants. This is the consequence of the distortion of the atomic surfaces in the approximant lattices.

The existence of distorted and low-symmetry clusters and the symmetry breaking by a different site occupancy may be understood in terms of the geometry of the atomic surfaces: To each coordination shell in the physical space $E_\parallel$ with atoms at the positions from the center (in appropriately scaled units), $\vec{R}_\parallel = \vec{n} + \vec{m}\tau$ (where $\vec{n}$ and $\vec{m}$ are vectors with integer or half-integer elements fixed by the geometry of the quasilattice) corresponds a coordination shell in perpendicular space $E_\perp$ with vectors $\vec{R}_\perp$ given by $\vec{R}_\perp = \vec{m} - \vec{n}\tau$. If not all points of the coordination sphere in $E_\perp$ fall inside the acceptance domain, their projections do not appear in $E_\parallel$ and the corresponding shell is incomplete. If the coordination sphere in $E_\perp$ intersects the boundary between the subshells of the acceptance domain, a mixed chemical occupancy of the corresponding shell in $E_\parallel$ follows. The bc_0-type Pd site has a special symmetry: in the quasiperiodic limit, where the center of the acceptance domain coincides with the bc_0 position in $E_\perp$, the distortions of the coordination shells from icosahedral symmetry disappear. For all other sites that are projected from off-center positions in $E_\perp$, low-symmetry coordination shells will exist also in the quasiperiodic limit, because the center of the coordination sphere in $E_\perp$ does not coincide with the center of the acceptance domain. A more detailed discussion of the atomic-shell structure of models produced by the cut-and-projection method from 6D space will be given elsewhere.[49]

D. Reciprocal quasilattices

Many discussions of structure-induced features in the electronic or vibrational spectra of quasicrystals are based on the concept of Brillouin zones, generalized in a vague way to quasicrystals. Niizeki[50,51] has shown how this generalization may be based on firm ground: To the 6D hypercubic lattice L_6 in the 6D space E_6 corresponds a 6D reciprocal lattice $L_6^\star$ (again hypercubic) in the 6D reciprocal space $E_6^\star$. A 6D Brillouin zone may be defined in the usual way; it is bounded by the planes bisecting the 6D $\mathbf{Q}$ vectors belonging to the star of equivalent 6D reciprocal lattice vectors. Special (high-symmetry points) corresponding to the Γ point at the center and the $X_2, M_2, X_3, M_3, X_5, M_5$, and R points at the 6D zone boundaries are defined by the representative vectors (with $h = \frac{1}{2}$) (000000), (hh0000), (0000hh), (hhh000), (000hhh), (h00000), ($hhhhh$0), and ($hhhhhh$). Their point-group symmetry is I_h for Γ and R, and D_{2h}, D_{3d}, and D_{5d} for X_i and M_i, depending on whether the subscript i is 2, 3, or 5. The projections of the 6D special points onto the 3D reciprocal space define sets of quasiperiodically distributed special points. The special points are dense everywhere, but with intensities modulated by interference effects and described by a generalized structure factor.[51] For the Γ points, the generalized structure factor reduces to the conventional structure factor. Figure 9 shows the intensities of the Γ points in a plane containing the twofold, threefold, and fivefold axes, calculated for the 5/3 approximant to i-Al-Pd-Mn. Similar plots may be constructed for the other special points. These quasiperiodically distributed sets of zone-center (Γ) and zone-boundary points (X_i, M_i, R) define the quasiperiodic analog to the extended-zone scheme of a crystal and provide a firm basis for the extension of the

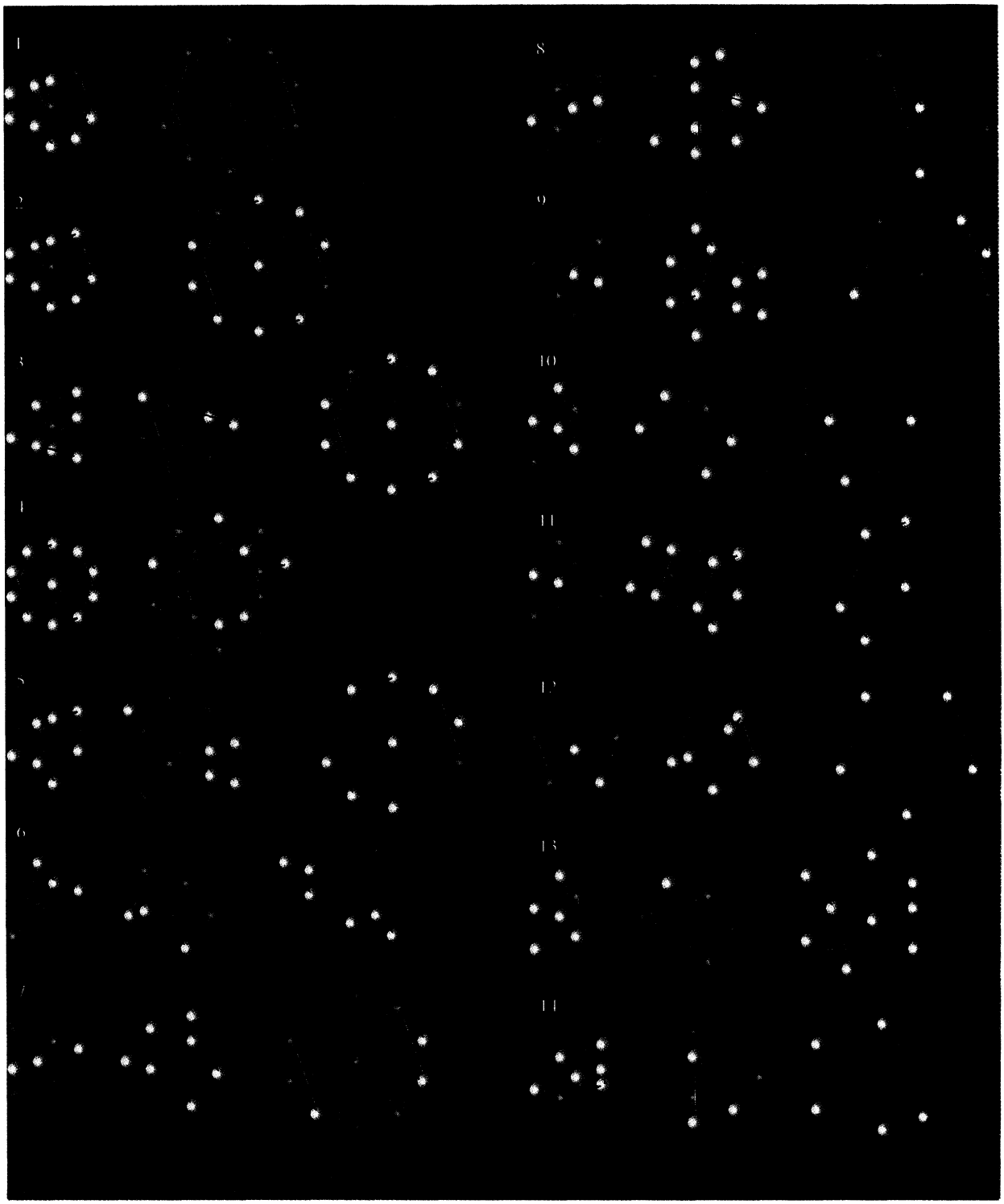

FIG. 7. Coordination shells for the 14 crystallographically inequivalent sites in the 1/1 approximant to *i*-Al-Pd-Mn. Yellow — Al atoms; blue — Pd atoms; red — Mn atoms. The green lines connect the vertices in each shell with exactly the same distance from the central atoms; atoms not connected by green lines are situated at a slightly different distance. Cf. text.

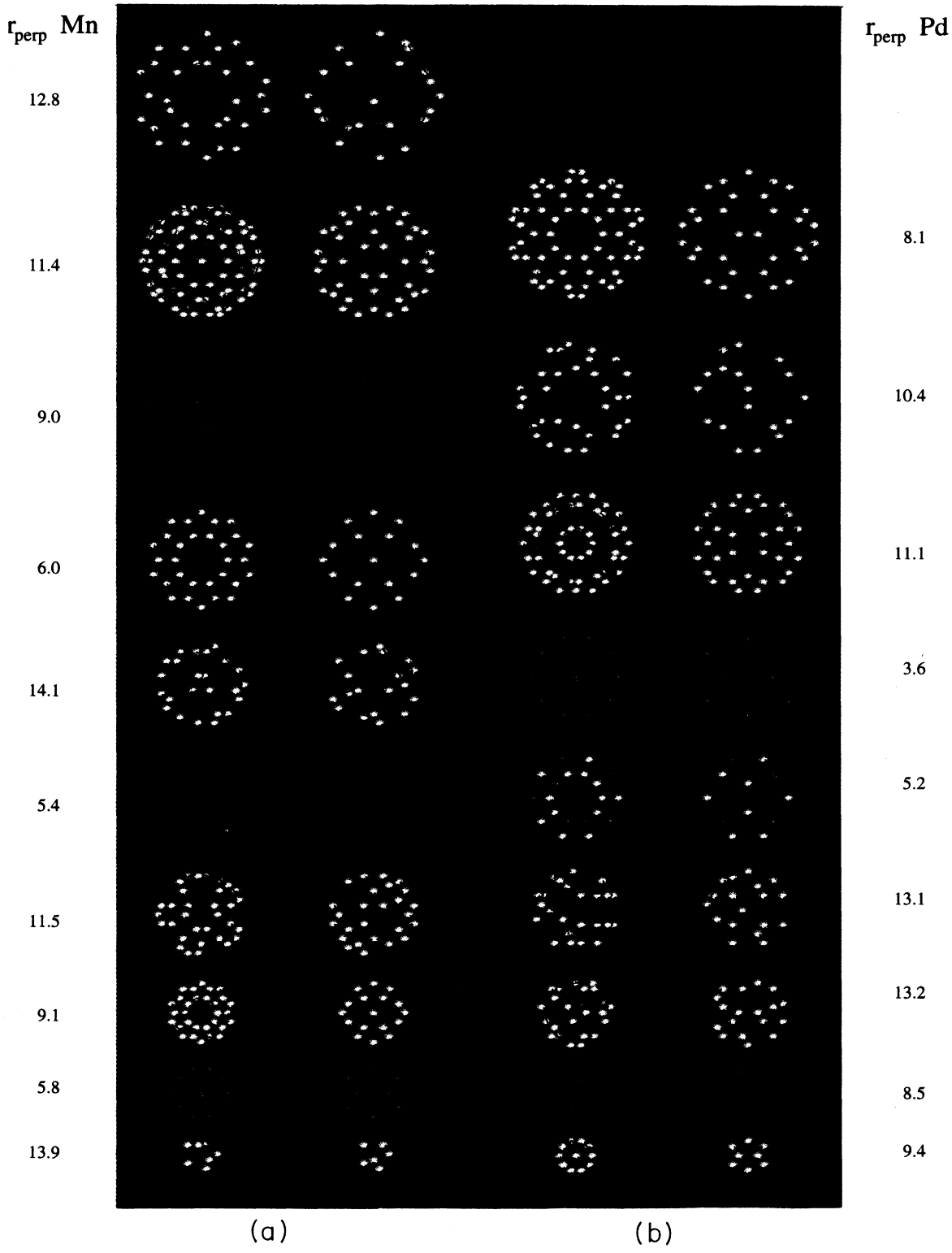

FIG. 8. (a) Coordination shells around a sevenfold Mn site in the 5/3 approximant to *i*-Al-Pd-Mn. The numbers listed give the number of the coordination shell and the radius of the corresponding shell in $E_\perp$ (in units of the lattice constant of the cubic lattice in $E_\perp$). The colors have the same meaning as in Fig. 7. See text. (b) Coordination shells around the bc_0 (twelvefold) Pd site in the 5/3 approximant to *i*-Al-Pd-Mn. For explanation of symbols, see Figs. 7 and 8(a).

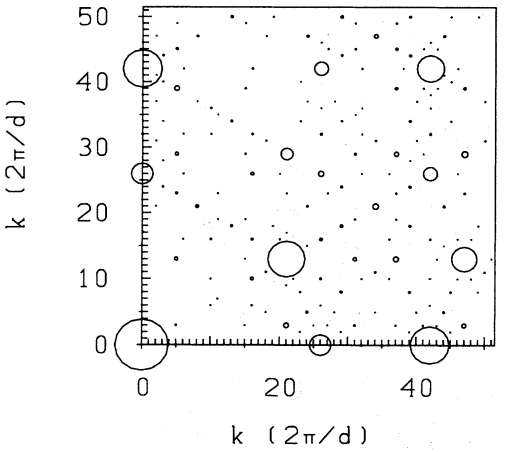

FIG. 9. Distribution and intensities of Bragg-peaks (≡ Γ-points) in a plane containing the twofold, threefold, and fivefold symmetry axes, calculated for the 5/3 approximant to icosahedral Al-Pd-Mn.

Brillouin-zone concept for the formation of band gaps to quasicrystals. Quasi-Brillouin zones may be defined in terms of the most intense zone-center and zone-boundary special points.

III. *AB INITIO* MOLECULAR-DYNAMICS CALCULATION OF THE ELECTRONIC STRUCTURE AND STABILITY OF THE 1/1 APPROXIMANT

To test the stability of a crystalline structure, one has to minimize the total energy with respect to the structural parameters. At least for the 1/1 approximant, such a calculation is now possible using *ab initio* density-functional molecular dynamics (MD) on the Born-Oppenheimer surface.[42,43,52] The principles of the technique are the following: The electronic ground state is calculated self-consistently in a plane-wave basis via a band-by-band minimization of the expectation values of the Kohn-Sham Hamiltonian using preconditioned conjugate-gradient techniques and efficient techniques[42,43] for charge-density mixing. The electron-ion interaction is described by optimized pseudopotentials. We use optimized norm-conserving pseudopotentials[53,54] for Al and ultrasoft pseudopotentials[53,55] for the transition-metal atoms Mn and Pd. For the ground state, the forces acting on the atoms can be calculated via the Hellman-Feynman theorem and corrections for the Pulay-forces arising from the augmentation charges of the ultrasoft pseudopotentials. With the known forces, the structure can be optimized via a quasi-Newton quench[56] under the constraint that the space-group symmetry is preserved.

We have applied the *ab initio* MD technique to the cubic 1/1 approximant (model $M2$) to the F-type icosahedral $Al_{88}Pd_{20}Mn_{20}$ quasicrystal with $P2_13$ symmetry and 128 atoms in the cubic cell (see Table I). Since we are interested mainly in the forces on the atoms and the equilibrium structure, the calculation has been performed only for the Γ point of the Brillouin zone. Convergence of the Brillouin-zone integrals is improved by using a Gaussian broadening of the one-electron energies within a finite-temperature density-functional theory.[42,43] For a cell with 128 atoms, this is certainly sufficient for a total-energy calculation, although perhaps not to resolve the finer details of the electronic spectrum. The minimization of the energy leads to only very small displacements from the sites of the idealized lattice (see Fig. 10). For most atomic sites, the displacements from the ideal lattice induced by the quantum many-body forces acting between the atoms are smaller than 1% of the average interatomic distance. The exceptions are the larger displacements of the Al atoms at the sites of type 10, 13, and 14 (see Fig. 7) amounting to ~ 4.5%, 2.5% , and 2%. However, even for these sites in a rather loosely packed low-symmetry environment, the calculated displacements are of the order of the thermal displacement amplitudes. Hence, they correspond only to small modifications of the atomic surfaces. This is confirmed by the comparison of the x-ray diffraction patterns of the ideal and the relaxed lattice (Fig. 11).

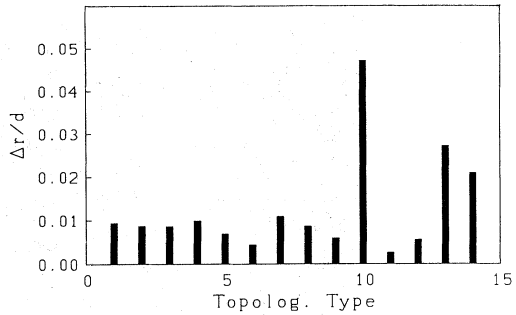

FIG. 10. Atomic displacements arising from the *ab initio* molecular-dynamics relaxation of the 1/1 ($M2$) approximant $Al_{88}Pd_{20}Mn_{20}$, plotted for the 14 crystallographically inequivalent sites.

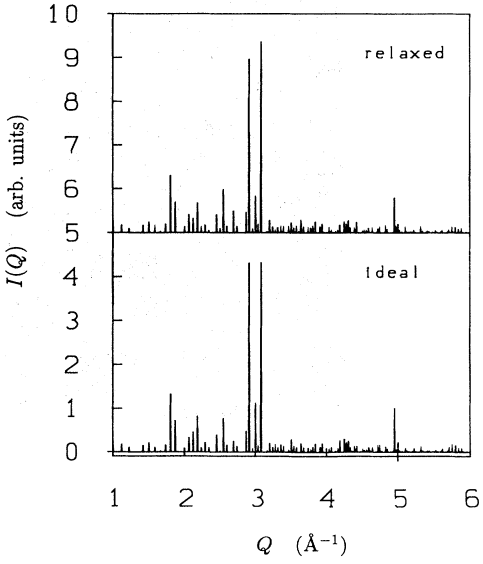

FIG. 11. X-ray powder-diffraction patterns calculated for the ideal (a) and the relaxed 1/1 ($M2$) approximant $Al_{88}Pd_{20}Mn_{20}$.

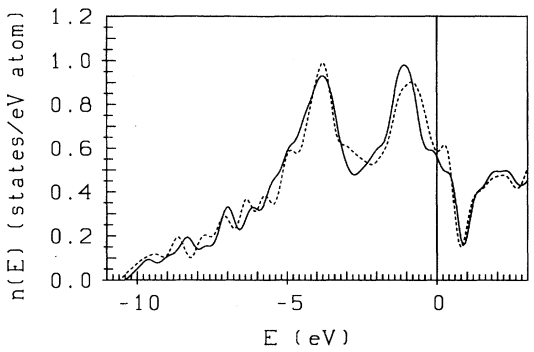

FIG. 12. Electronic density of states of the relaxed 1/1 ($M2$) $Al_{88}Pd_{20}Mn_{20}$ approximant, calculated via *ab initio* density-functional MD. Full lines — relaxed model, broken lines — ideal model.

The self-consistent electronic density of states for the ideal and relaxed models is shown in Fig. 12. The lower part of the valence band has the parabolic form expected for an essentially free-electron-like Al band, structured by the complex atomic structure. The DOS maxima at binding energies of 4 eV and 1 eV arise from the Pd- and Mn-d states, respectively. The Fermi-level falls into a region of decreasing DOS, a very deep minimum is found 0.8 eV above E_F. The DOS minimum is induced by the strongest Bragg-peaks in the diffraction pattern, it is not affected by the structural relaxation. We discuss the significance of the DOS minimum in more detail in the next section.

IV. LINEAR-MUFFIN-TIN-ORBITAL CALCULATIONS OF THE ELECTRONIC STRUCTURE OF THE 1/1 AND 2/1 APPROXIMANTS

The pseudopotential-based *ab initio* MD technique gives the probably most accurate electronic structure of compounds that are as complex as the approximants to icosahedral structures. However, at present a cell with 128 atoms (comprising transition atoms) is close to the maximum that can be handled even with the softest pseudopotentials and with the most sophisticated techniques for iterative matrix diagonalization. For the higher-order approximants, we have to adopt a method that allows for a transformation to a localized basis and for the use of real-space Greens-function techniques for the calculation of the electronic spectrum. The basis of our approach is the self-consistent calculation of the electronic structure of the low-order approximants using the LMTO approach in the scalar relativistic atomic-sphere approximation (ASA).[41] The radii of the atomic spheres for the different chemical species ($R_{Al} = 1.56$ Å, $R_{Pd} = 1.55$ Å, $R_{Mn} = 1.46$ Å) are chosen such as to match the ratio of the nearest-neighbor distances. The use of the ASA for a structure with coordination numbers as low as those of the Al-Pd-Mn quasicrystals (cf. Table II) and local environments of low symmetry might be considered as questionable, because of the muffin-tin form of the potential. Here the possibility to compare the results with those of the *ab initio* MD calculations in a plane-wave basis is a very important test.

The extension to the higher-order approximants is based on the transformation of the Hamiltonian from the LMTO basis to the most localized tight-binding basis.[44] Details of the application of the TB-LMTO formalism to quasicrystalline approximants are given in our previous papers.[10,11] The LMTO structure constants are calculated for each atomic site, including all neighbors within a sphere of radius $R_{cut} = 2.68 \times \overline{R}_{WS}$ ($\overline{R}_{WS}$ is the average Wigner-Seitz radius of the atomic spheres) containing on average 20 atoms. The two-center TB Hamiltonian in the Löwdin orthonormal representation is determined in terms of an expansion in powers of the nonorthogonal TB Hamiltonian in the screened, most localized basis and the overlap matrix. This expansion is truncated at the second-order term. Since (within the spatial extension of the most localized TB-LMTO's) the local atomic environments of the lowest-order approximants are also found in the higher-order phases, a very good approximation to the TB-LMTO Hamiltonian is obtained by using the self-consistent local potential parameters for the 1/1 phase, averaged over the sites of each chemical species.

For the 1/1 phase, we calculate electronic eigenvalues and eigenfunctions on a rather fine mesh in $\vec{k}$ space (up to 24 points in the irreducible part of the Brillouin zone) and perform $\vec{k}$-space integrations using the linear tetrahedron method.[57] The Hamilton matrix is diagonalized repeatedly for each $\vec{k}$ point until self-consistency has been achieved. The use of a fine $\vec{k}$-space mesh allows us to resolve the fine structure of the electronic spectrum at a scale of 10^{-2} eV. For the 2/1 approximant with 544 atoms, even with the minimal s,p,d basis the dimension of the Hamilton matrix is 4896 × 4896, and a straightforward diagonalization is not possible. At the high-symmetry points of the Brillouin zone, however, we can use the $P2_13$ symmetry of the lattice to reduce the Hamiltonian to block-diagonal form. The space-group $P2_13$ has one one-dimensional real, one one-dimensional complex, and three three-dimensional representations, so that at the Γ point the Hamiltonian can be reduced to blocks with a maximum size of one-fourth of the dimension of the full Hamilton matrix. For points of lower symmetry, the block diagonalization does not lead to a sufficient reduction of the size of the Hamilton matrix. In practice, we use only the Γ point, so that we cannot really improve the resolution of the spectrum beyond that achieved for the 1/1 approximant. However, the diagonalization of the block-diagonal Hamiltonian allows us at least to calculate the electronic eigenfunctions of the 2/1 approximant in the TB-LMTO basis and to study the behavior of the wave functions beyond the lowest-order approximant.

A. Electronic structure of the 1/1 approximant

Figures 13 and 14 show the total and partial Al, Pd, and Mn densities of states and the integrated total densities of states for the $M1$ and $M2$ models of the 1/1 ap-

proximant. The $M1$ model with the low Mn and high Pd content ($Al_{88}Pd_{32}Mn_8$) shows an Al band with a width W of 10.3 eV that is only slightly lower than that in pure crystalline Al ($W = 11.4$ eV). Note that the bandwidth is almost the same (to within $\pm$ 0.2 eV) as in all other icosahedral phases: $W = 10.5$ eV in i-Al-Zn-Mg (Ref. 10), $W = 10.2$ eV in i-Al-Cu-Li (Ref. 11), $W = 10.2$ eV in i-Al-Cu-Fe (Ref. 58), with the exception of $W = 12.2$ eV in i-Al-Mn (Ref. 59). Although the structure of the band is dominated by many sharp spikes, its form is essentially free-electron-like (parabolic) near the bottom and shows a broad depression around the Fermi level. The Pd band is about 3 eV wide and centered at a binding energy of $E \sim 4.2$ eV ($M1$) and $E \sim 3.8$ eV ($M2$), respectively, the broad Mn-band has its maximum about 0.8 eV below the Fermi energy. This means that compared to pure Pd metal, the peak in the d-band DOS is shifted by about 2.8 eV to higher binding energies. This d-band shift is also a generic property of crystalline and amorphous alloys of early and late transition metals, it arises from the covalent interaction between the d states in a nearly full and in a half-filled band.[60–62] Because of the low Pd and Mn concentrations and the chemical order (complete absence of direct Mn-Mn neighbors, cf. Table I and Fig. 7), both the Pd- and the Mn-d bands have the character of impurity bands and lack the pronounced bonding–antibonding splitting that characterizes the transition-metal d bands.

The results of the LMTO calculations compare very well with the *ab initio* pseudopotential calculations, considering the much finer $\vec{k}$ mesh used in the LMTO calculations. This point is important since it confirms that the use of the ASA is adequate even for the relatively low coordination numbers of the approximant phase.

Close to E_F, one finds a number of very deep and narrow pseudogaps, but the DOS at E_F is relatively high. The DOS for the $M2$ model ($Al_{88}Pd_{20}Mn_{20}$) shows two maxima from the Pd- and Mn-d bands at $\sim$ 3.8 eV and $\sim$ 0.8 eV binding energy. The most striking feature consists in several very deep and narrow gaps immediately around E_F. The most pronounced gap is found 0.6 eV above E_F. It is interesting that this gap occurs precisely at the band filling of five electrons per atom corresponding to the exact composition of the quasicrystal. Hence the electronic spectrum reflects the conflicting requirements for the construction of an energetically favorable 1/1 approximant: Model $M2$ has the correct topology leading to the formation of a strong structure-induced pseudogap in the electronic DOS, but because of the wrong chemical composition, the Fermi level falls below the gap so that the electronically driven stabilization is

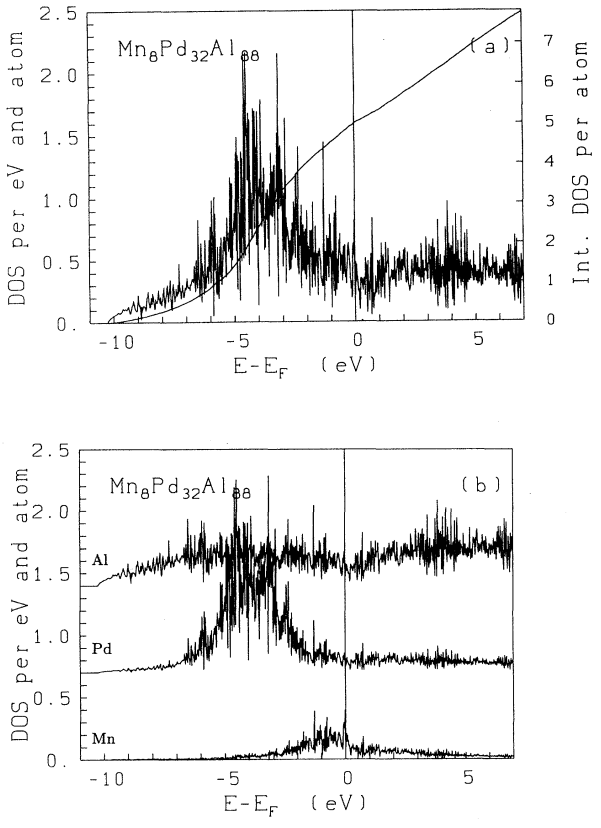

FIG. 13. Total differential and integrated densities of states (a) and average local electronic density of states on the Al, Pd, and Mn sites (b) of the 1/1-approximant $Al_{88}Pd_{32}Mn_8$ (model $M1$), calculated using the LMTO-ASA.

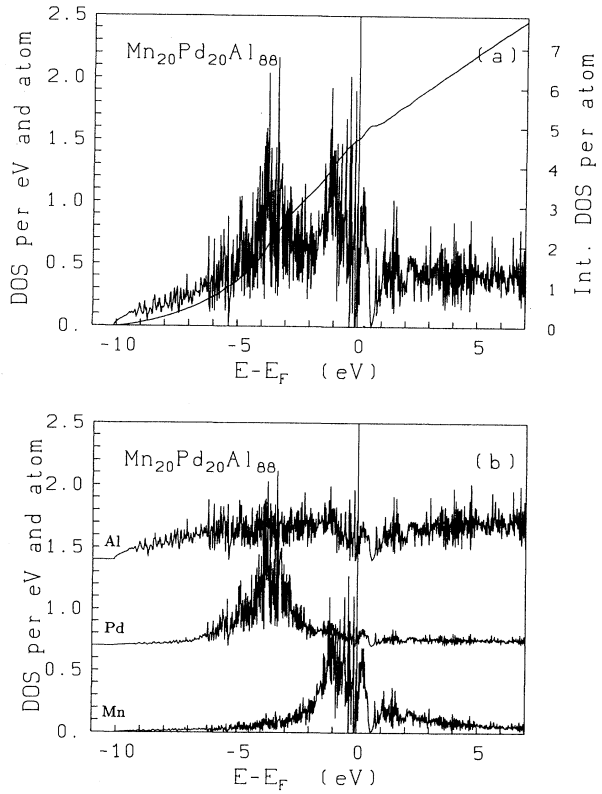

FIG. 14. Total differential and integrated densities of state (a) and average local electronic density of states on the Al, Pd, and Mn sites (b) of the 1/1-approximant $Al_{88}Pd_{20}Mn_{20}$ (model M2), calculated using the LMTO-ASA.

not effective. Model $M1$ where the atomic surfaces have been adjusted such as to produce the correct stoichiometry does not possess the correct topological order leading to a sufficiently strong pseudogap.

The electronic mechanism for the stabilization of the quasicrystalline phase has often been discussed in terms of critical Hume-Rothery-type electron/atom ratios.[13] Assigning to the transition-metal atoms the negative valencies calculated by Raynor[63] (Mn $Z = -4.66$, Pd $Z = -0.62$), a critical electron/atom ratio per Al atom of e/A $\sim$ 1.7–1.8 is derived for the stable icosahedral Al-Cu-TM, Al-Ni-TM, and Al-Pd-TM phases. Our results do not support this argument. For the 1/1-$M2$ approximant $Al_{88}Pd_{20}Mn_{20}$, we find that the atomic spheres are almost exactly neutral (Al $\Delta Z \sim -0.04$, Mn $\Delta Z = 0$, Pd $\Delta Z = 0.15$). This excludes a picture claiming that the transition metals bind some of the Al-valence electrons, leading to a reduced effective valence for Al placing the Fermi energy in the gap. The narrowing of the Al band has to be attributed to the hybridization with the Pd- and Mn-d states.

It is also interesting to examine the local DOS at the crystallographically inequivalent sites (see Figs. 7 and 15 for model 1/1-$M2$). The structure-induced gap above E_F is visible at all sites, most distinctly for the three Mn sites where it cuts deeply into a region of high DOS. In the local Mn DOS's, we also find a number of very narrow gaps at very small distance from the Fermi level. There are considerable differences in the local DOS on the three Pd sites, depending mainly on the existing Pd-Mn correlations: at the bc_0 Pd site, besides the main Pd-d peak at -3.8 eV below the Fermi level there is a Pd-p peak at the Fermi level, arising mainly from the interactions with the Pd and Mn atoms in the second shell surrounding the bc_0 site (cf. Fig. 7). This side peak of p character persists also in the higher-order approximants, despite the change in the local chemical order [cf. Fig. 8(b) and below]. The differences in the DOS's on the two other Pd sites arise again from different Pd-Mn coordinations. The high DOS between E_F and -1 eV at site 6 arises from the strong interaction of the central Pd atoms with four Mn atoms at short distances. Again, in all local DOS's, narrow gaps exist around E_F. In the local Al-DOS's, the sharp structure-induced gaps are embedded in a broad depression around E_F, which has its origin in the hybridization with Mn-d states. Similar structures at higher binding energies arise from the hybridization with Pd-d states at some of the Al sites.

B. Electronic structure of the 2/1 approximants

The total electronic DOS of two models for the 2/1 approximant, calculated in terms of the distribution of the eigenvalues at the Γ point, folded with a Gaussian of width 0.025 eV, is shown in Fig. 16. Note that model $M1$ is closest in composition to the 2/1 approximant reported by Waseda *et al.*[40] (5.88 at. % Mn against 4 at. %). The overall form of the DOS is rather similar to that found for the 1/1 approximant with the correct chemical composition ($M1$), with a number of narrow DOS minima around the Fermi energy. The deepest minima are found 0.6–0.8 eV above E_F. Note that the composition reported by Waseda *et al.* corresponds to a higher filling of the band, so that the Fermi energy would fall closer to the DOS minimum. This is again a hint to the importance of the electronic mechanism for stabilizing the quasiperiodic and approximant phases.

It is also interesting to observe the change in the fine structure in the DOS on going from the 1/1 to the 2/1 approximant. It appears that the DOS of the 2/1 approximant is even more structured than that of the 1/1 phase. However, we have to keep in mind that it is computationally not feasible to take the $\vec{k}$-space grid to convergence: a finer grid would show additional fine structure, but reduce the amplitude of the fluctuations in Fig. 16.

V. TB-LMTO RECURSION APPROACH TO THE ELECTRONIC STRUCTURE OF THE HIGHER-ORDER APPROXIMANTS

For the 3/2 and all higher-order approximants, a diagonalization of the Hamiltonian is no longer possible (one could, in principle, proceed by iterative calculation of the lowest eigenvalues via conjugate-gradient techniques. However, even for the 5508 occupied eigenvalues of the $20\,628 \times 20\,628$ Hamilton matrix of the 3/2 approximant, the computational effort is prohibitively large). Therefore, we decided to use the real-space recursion technique of Heine *et al.*[64] for the calculation of the total and partial DOS and for the Bloch spectral functions. The real-space recursion technique calculates, in principle, a density of state $n_\psi(E)$ projected onto an initial state $|\psi\rangle$ via a continued fraction representation of the diagonal matrix element $G_{\psi\psi}(E)$ of the Greens function $G(E) = (E - H + i0^+)^{-1}$. If the initial state $|\psi\rangle$ is a random unitary vector, the resulting DOS is the total density of states $n(E)$, a possible statistical error may be minimized by taking an average over a set of random vectors. Partial and local DOS's may be obtained by restricting the initial state to certain sites or angular-momentum components. If the initial state is a plane wave propagating in a direction $\vec{k}$, the resulting projected DOS is a Bloch spectral function $f(\vec{k}, E)$. In practice, the continued fraction has to be terminated at a level L much smaller than the dimension N of the Hamilton matrix. A smooth density of states is obtained by using a proper terminator (i.e., using an algorithm that performs an analytic extrapolation of the continued fraction to infinity). In our calculations, we used 20, 40, 60, 80, and 130 recursion levels for the 1/1, 2/1, 3/2, 5/3, and 8/5 approximants with periodic boundary conditions (for the lowest-order approximants, we use supercells consisting of 27 and 8 unit cells, respectively, as the basic units for the recursion calculations), Gaussian-quadrature termination[65] for the DOS and the Lucchini-Nex terminator[66] for the calculation of the Bloch spectral functions. Note that with 130 recursion levels and a bandwidth of about 15 eV (including empty states), the estimated resolution in energy is $\sim$ 0.15 eV for the 8/5 approximant.

A. Total and partial densities of state

Figure 17 shows the variation of the total DOS through the hierarchy of the approximants, from the 1/1 approximant with 128 atoms to the 8/5 phase with 41 068 atoms. We find two essential trends: (i) The characteristic pseudogap just above E_F shifts closer to the Fermi edge in the higher-order approximants. In the 3/2 to 8/5 approximants, it occurs exactly at the Fermi energy. The depth of the pseudogap, however, does not depend on the order of the approximant. The calculated DOS at the Fermi energy of $n(E_F) = 0.31$ eV/states atom is significantly

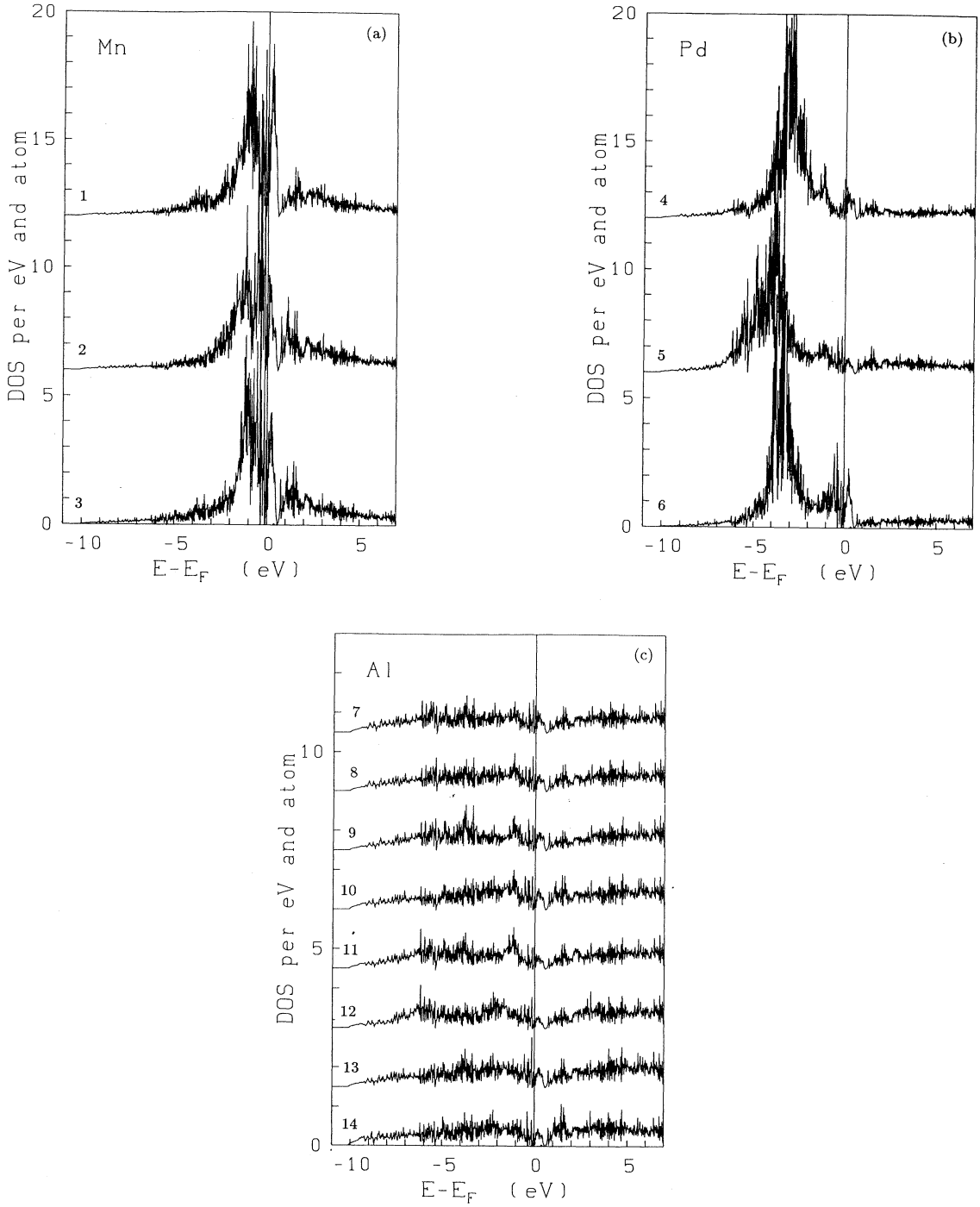

FIG. 15. Local electronic density of states on the 14 crystallographically inequivalent sites in the 1/1-approximant $Al_{88}Pd_{20}Mn_{20}$. (a) Mn sites, (b) Pd sites, (c) Al sites. The local DOS's should be compared with the local atomic environments shown in Fig. 7; the same number is used to distinguish the crystallographically inequivalent sites.

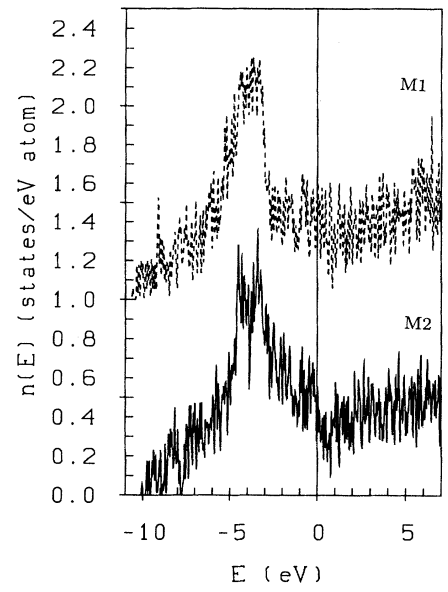

FIG. 16. Total electronic density of states of the two versions of the 2/1 approximant to i-Al-Pd-Mn: $Al_{372}Pd_{124}Mn_{48}$ (full lines) and $Al_{372}Pd_{140}Mn_{32}$ (broken lines), calculated by diagonalizing the Hamilton matrix at the Γ point. Cf. text.

lower than the free-electron DOS of pure Al [$n(E_F)$ = 0.365 states/eV atom], but not quite as low as the experimental value of $n(E_F) = 0.174 \pm 0.05$ states/eV atom reported by Chernikov *et al.*[34] The limited resolution of the recursion calculation which tends to smear out fine structure in the DOS might be responsible for at least

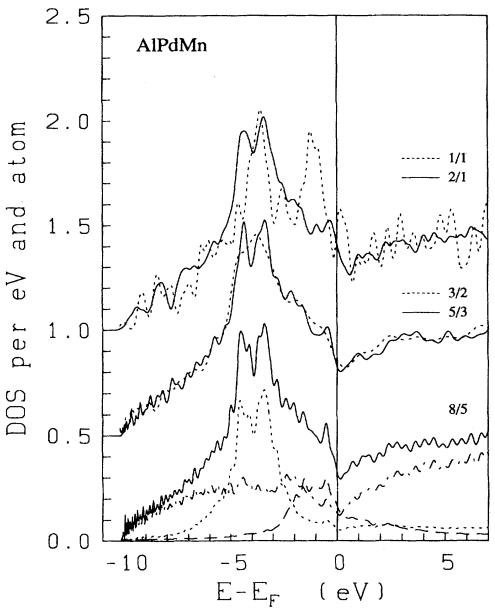

FIG. 17. Total electronic densities of states of the 1/1(M2) to 8/5 approximants to i-Al-Pd-Mn, calculated using the TB-LMTO recursion method. For the 8/5 approximant, we show in addition the local Al (dashed lines), Pd (dotted lines), and Mn DOS (dot-dashed lines).

part of the discrepancy, as the measured values could correspond to the minimum in a gap that is narrower than our computational resolution. (ii) With increasing order of the approximant, the characteristic energy scale of the fine structure is reduced and the amplitude in the fluctuations in the DOS is reduced. To a certain degree this is the consequence of the improved resolution, due to the increased number of recursion levels. However, neither numerical calculations of the DOS nor spectroscopic experiments will be able to answer the question as to the character of the spectrum (continuous, singular, or singular continuous?) in the quasiperiodic limit. However, these changes do not affect the structure-induced pseudogap at E_F and its effect on the energetic stability.

The partial DOS's for the 8/5 approximant show that the Al-DOS converges to a parabolic nearly free-electron (NFE) form, superposed by a broad pseudogap around the Fermi level and many oscillations whose resolution is limited by the numerical details of the calculation. Both the Pd and Mn bands have a full width at half maximum of ~ 2.3 eV, i.e., they are much narrower than in the pure metals. The Pd band shows a weak bonding-antibonding splitting, but the resonance in the Pd-DOS close to the Fermi level is now very weak. This is a consequence of the variation of the local chemical order in the sequence of the approximants (cf. Sec. II C). In contrast to the 1/1-$M2$ approximant, there are only very weak indications for a pseudogap at E_F in the Pd and Mn bands.

We have also calculated the partial charges of the three chemical species. As for the 1/1 approximants, we find that charge-transfer effects are small, but the exact value depends to some degree on the assumed atomic-sphere radii. Again the narrowing of the Al band cannot be explained in terms of charge transfer from Al to the transition-metal atoms.

B. Dispersion relations and mechanism for band-gap creation

For the s,p-bonded quasicrystals of the Al-Zn-Mg and Al-Cu-Li classes, we have shown that the formation of a pseudogap may be understood in terms of a quasiperiodic nearly free-electron model and the concept of quasi-Brillouin-zone boundaries.[10,11] The NFE form of the Al band suggests that a similar mechanism could also help to explain the formation of the pseudogap in the DOS of i-Al-Pd-Mn. Figure 18 shows the Bloch spectral functions $f(\vec{k}, E)$ for wave vectors pointing in the direction of one of the twofold axes, calculated for the 5/3 approximant, Fig. 19 the dispersion relations for electrons (the "band structure"), defined in terms of the locations of peaks in $f(\vec{k}, E)$. At energies close to the bottom of the band, we find a series of sharply defined free-electron parabolas originating from the most intense Bragg peaks (i.e., from the most intense Γ points of the quasilattice, cf. Fig. 9). Around 4 to 5 eV binding energy, we find a series of somewhat broader peaks representing the Pd states. Again these peaks are most pronounced close to the Γ points where also the splitting into a bonding and

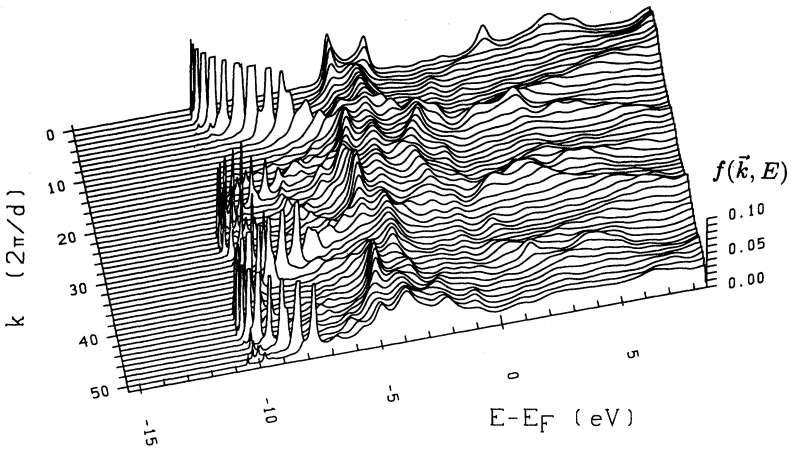

FIG. 18. Bloch spectral functions $f(\vec{k}, E)$ (in arbitrary units) for the 5/3 approximant to i-Al-Pd-Mn and for wave vectors oriented along one of the twofold symmetry axes.

an antibonding peak is largest. Halfway between the Γ points (i.e., close to the quasi-BZ boundaries), a single peak at lower binding energy dominates. The Mn-derived peaks at 1 to 2 eV binding energies are also most intense at the quasi-BZ boundaries.

The dispersion relations given in Fig. 19 show that close to the bottom of the valence band, the dispersion of the Al-s states follows very closely a set of quasiperiodic free-electron parabolas. A similar result is found for wave vectors pointing into the fivefold and threefold directions. Close to the Fermi energy, one finds a quasiperiodic set of degenerate free-electron states at the "quasi-BZ boundary" points (the X_2 and M_2 points along the twofold symmetry axes). As in the s,p-bonded quasicrystals,[10,11] the electron-ion interaction leads to the formation of gaps close to the Fermi energy. These gaps exist at all wave vectors (see the valley in the spectral functions in Fig. 18), but they are most pronounced at the most intense X_2 and M_2 points (which are in turn connected to the most intense Γ points by free-electron parabolas). Due to the high symmetry of the icosahedral phases, the distribution of the gaps is isotropic in $\vec{k}$ space. The dispersion of the Pd- and Mn-d states is much weaker and does not interfere with the structure-induced formation of pseudogaps in the Al bands.

It is also interesting to point out that the intensities of the nearly dispersionless d states, and especially that of the Mn-d states close to the Fermi level is highest at the "quasi-Brillouin-zone" boundaries. It is well known that there is a correlation between the absence of dispersion and the localization of eigenstates. The possibility of a localization (or confinement) of the Mn states close to E_F will be discussed further in Sec. VII.

C. Atomic-shell structure and electronic properties

In view of the often claimed importance of the existence of well-defined icosahedral clusters, we wanted to explore the electronic properties of the clusters that we have identified in the Al-Pd-Mn phase. First, we look at the local DOS at the Pd atom in the central bc_0 position. Figure 20 shows the local DOS calculated for clusters of increasing size, starting with a cluster of 57 atoms consisting of the central Pd site, an inner icosahedron of Al atoms, a pentagonal dodecahedron of Pd atoms, and an irregular polyhedron with 24 Al atoms (see Sec. II C), and adding further shells as the size of the cluster increases. The calculations have been performed with the recursion technique and 20 recursion levels. We find that the addition of a fourth and fifth shell to the cluster (bringing the total number to 101 atoms) still introduces substantial changes in the local DOS at the central site, especially around the Fermi level. Further layers leave the local DOS with a broad band of d levels centered around 3.5 eV binding energy and a relatively sharp p resonance at the Fermi level almost unaffected, except for the sharp features close to the bottom of the band which disappear only after adding the tenth shell of atoms (compare also with the partial Pd-DOS in Fig. 17). We conclude that we have to use clusters with a minimum of $\sim 200-250$ atoms to obtain a reasonable approximation to the quasicrystalline local DOS at the central site.

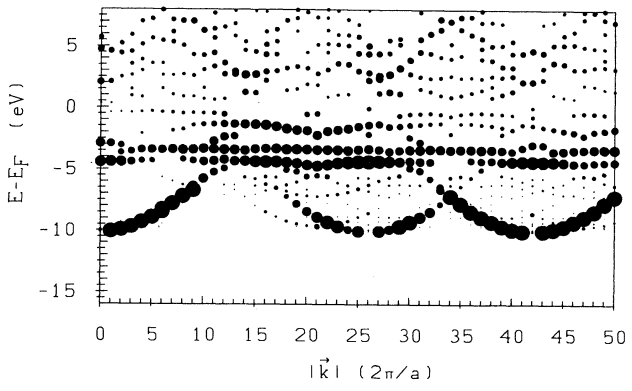

FIG. 19. Dispersion relations $E(\vec{k})$ for electrons in the 5/3 approximant to i-Al-Pd-Mn for $\vec{k}$ points along a twofold symmetry axis. The full points indicate a peak in the Bloch spectral function, the size of the dot scales with the amplitude of the peak.

In the next step, we consider the local DOS's on the successive atomic shells around the bc_0-Pd position [cf. Fig. 8(b) for a graphical representation]. Again, we use the recursion method with 20 levels, applied to a cluster of 413 atoms for the inner shells and 1099 atoms as we approach the outer coordination shells. The DOS on the central Pd site agrees with the converged result in Fig. 20. The first icosahedral Al shell is characterized by a very broad and deep DOS minimum around the Fermi level (see Fig. 21). The second dodecahedral shell of Pd atoms also shows a DOS minimum at E_F. Shells 3 and 4 consist of irregular Al polyhedra and show again the deep pseudogap. The dodecahedral (τ-scaled) shell 5 has a mixed occupation of Al and Mn. The Al local DOS has again the pseudogap (enhanced by the hybridization of the Al states with the Mn states in the neighboring shells), but the local Mn DOS, as well as the Mn DOS of the icosahedral τ^2-scaled sixth shell show a high DOS at the Fermi level. The seventh (pure Al), eighth (mixed Al and Pd), and ninth (pure Al) shells display again the characteristic DOS minimum at E_F. The tenth shell (Mn,Pd) has a large maximum in Mn-d DOS and a local minimum in the Pd-d DOS at the Fermi level, it is followed by a Al shell with a very broad and a more narrow pseudogap (only the local DOS up to the eighth shell are displayed in Fig. 21). The variation of the width and depth of the pseudogap at E_F in the Al-DOS shows that the formation of the gap is enhanced by the hybridization of the Al states with the d states of the transition metals in the neighboring shells.

Finally, we analyze the electronic structure of the Mn-centered clusters shown in Fig. 8. The first 7-atom and the third 30-atom Al shells show again the deep pseudogap, evidently induced at least in part by the hybridization with the central Mn-atom and the 12 Mn atoms in the second icosahedral shell (see Fig. 22). The pseudogap effect is weaker in the more distant Al shells, whose sequence is interrupted only by the 7-atom Pd shell. Stronger pseudogap effects are found again in the 10th and 12th Al shells that bracket a pentagonal dodecahedron of Mn atoms (not shown).

The conclusion to be drawn from this investigation is twofold: (i) The hybridization of the Al states with the transition-metal d states (especially with the Mn-d band) is important for the formation of the pseudogap at the Fermi level. (ii) Neither the structural analysis nor the investigation of the electronic properties would justify an interpretation of the structure in terms of icosahedral clusters joined together by "glue atoms."

VI. PHOTOELECTRON AND SOFT-X-RAY SPECTRA

In this section, we confront the calculated electronic structure with spectroscopic experiments. The photo-

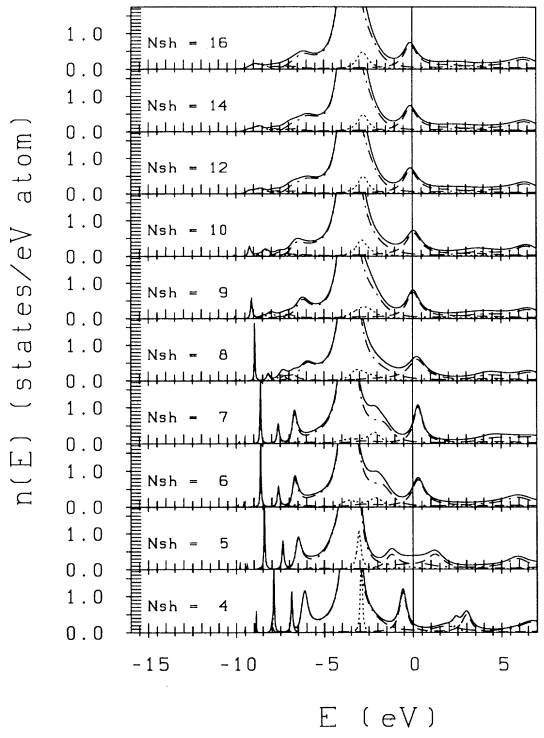

FIG. 20. Local DOS at the central bc_0 Pd position as a function of the increasing size of the surrounding cluster. The first DOS shows the result for the central 57-atom units, in each following DOS one more atomic layer is added to the cluster. See Fig. 8(b) and text.

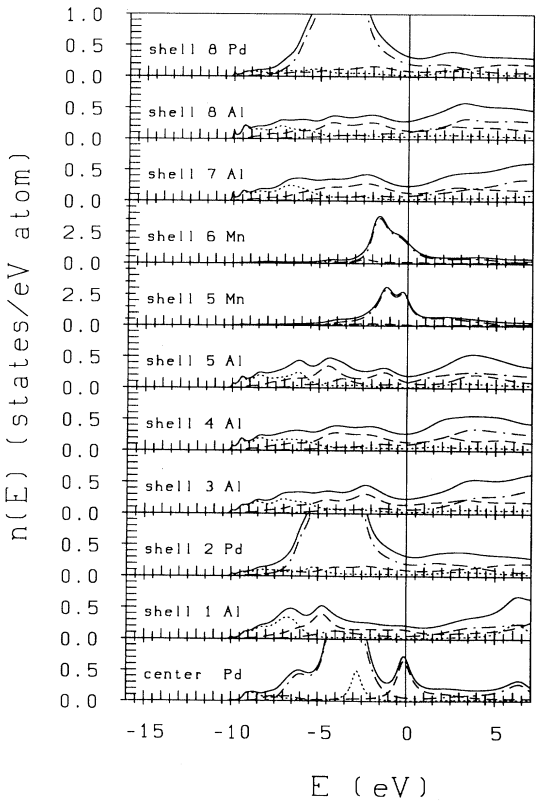

FIG. 21. Local DOS in the center and on the succesive coordination shells surrounding the bc_0 Pd site. Cf. Fig. 8(b) and text.

emission spectra of Zhang *et al.*[37] probe the occupied part of the valence band, the soft-x-ray absorption and emission spectra of Belin *et al.*[38] yield information about occupied and empty states. The advantage of the soft-x-ray spectra is to yield information on the partial DOS (or a combination of two partial DOS), due to the selection rules of the radiative transitions, albeit at a relatively low resolution that does certainly not allow to resolve narrow gaps in the DOS. The photoelectron spectra allow us to achieve better resolution, but represent averages over the partial DOS's weighted with the partial photoionization cross sections. Resonant photoemission exploits the strong variation of the cross section for an outershell electron with the energy of the exciting photon close to the value, where the excitation energy exceeds the threshold for an inner transition and allows us to ascribe certain features of the valence band to a particular chemical species.

A. Soft-x-ray spectroscopy

Figures 23(a–h) compare the x-ray emission spectra (a–d) and the x-ray absorption and photoyield spectra (e–h) with the calculated partial densities of states. The Al-p and Al-$(s+d)$ DOS's in the valence bands (VB) have been investigated using transitions from the VB to the $1s$ and $2p_{3/2}$ states, at energies around 1560 eV and 70 eV. The Mn- and Pd-$(d+s)$ DOS's have been probed, using the transitions from the valence band to the $2p_{3/2}$ level, at energies around 635 eV and 3170 eV, respectively. The differences in the excitation energies must be considered when comparing theory and experiment.

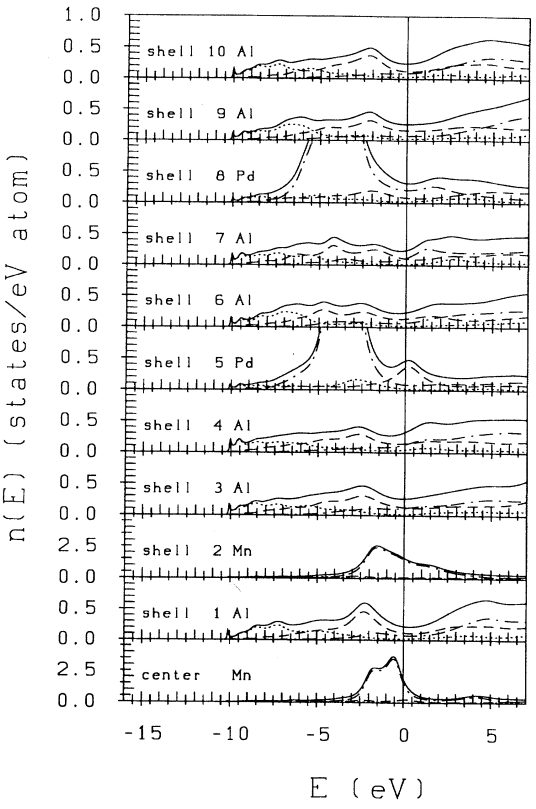

FIG. 22. Local DOS in the center and on the successive coordination shells surrounding a sevenfold Mn site. Cf. Fig. 8(a) and text.

The SXE spectra for Pd (c) and Mn (a) agree with our calculation in placing the maxima of the d bands at $E = 3.8 \pm 0.3$ eV (Pd) and $E = 0.8$ eV (Mn). For comparison with experiment, the calculated partial DOS's have been convoluted with a Gaussian of width $\sigma = 0.3$ eV to simulate the effects of instrumental resolution and lifetime broadening. Evidently, the effect of lifetime broadening is much stronger for the VB-$2p_{3/2}$ transition in Pd than in Mn — this explains the much larger width in the observed Pd-L_β spectrum. The Al-SXE spectra confirm the calculated width and shape of the Al-p (b) and Al-$(s+d)$ (d) DOS's very well. The difference in the relative heights of the two peaks in the Al-$(s+d)$ DOS arises from differences in the transition-matrix elements, for the s-p and d-p transitions that are not considered in the theoretical results approximating the spectrum by the combined $(s+d)$ partial DOS. The peak at higher binding energy is clearly to be associated with Al-s states, whereas the peak closer to the Fermi edge has stronger d character. The splitting of the two subbands is also enforced by the interaction with the Pd-d band.

For the SXA spectra, we find good agreement in shape and width for the Mn-$(s+d)$ (e) and Al-p (f) conduction bands, but a systematic shift in the position of the Pd-$(s+d)$ (g) and Mn-p (h) bands (whose form is otherwise

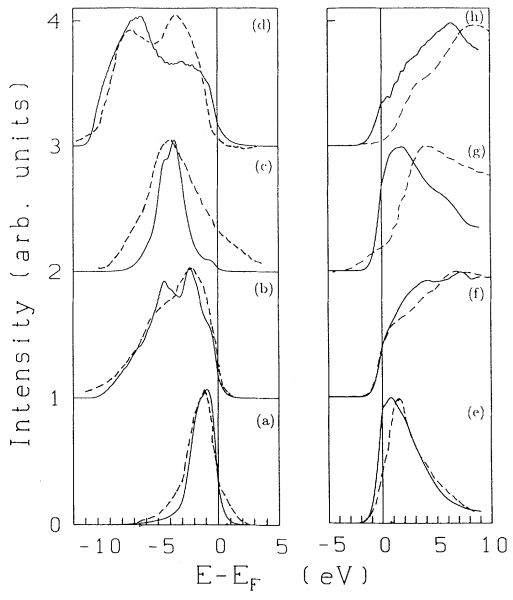

FIG. 23. Comparison of the soft-x-ray emission spectra (Ref. 38) with the calculated partial densities of states of the valence band: (a) Mn-$(s+d)$, (b) Al-p, (c) Pd-$(s+d)$, (d) Al-$(s+d)$. Comparison of the soft-x-ray absorption and photoyield spectra with the calculated partial densities of the conduction band: (e) Mn-$(s+d)$, (f) Al-p, (g) Pd-$(s+d)$, (h) Mn-p. For all spectra, the maximum intensity has been normalized to unity. Cf. text.

well predicted). At the present moment, we can only assume that the difference arises from an error in locating the experimentally measured intensity distribution relative to the Fermi level. This would also agree with the expected intensities of the Pd-$(s+d)$ states in the valence and conduction bands. Adjusting the intensity of the experimental SXE and SXA spectra for Pd [curves (c) and (g)] at the Fermi level would lead to a rather high Pd-d DOS in the conduction band, in evident contradiction to the fact that the Pd-d band is nearly completely filled. Except for this difficulty, we find that the predicted DOS is well confirmed by the soft-x-ray experiment. However, due to the rather low resolution, the experiment does not represent a critical evaluation of the prediction concerning the depth of the pseudogap at E_F.

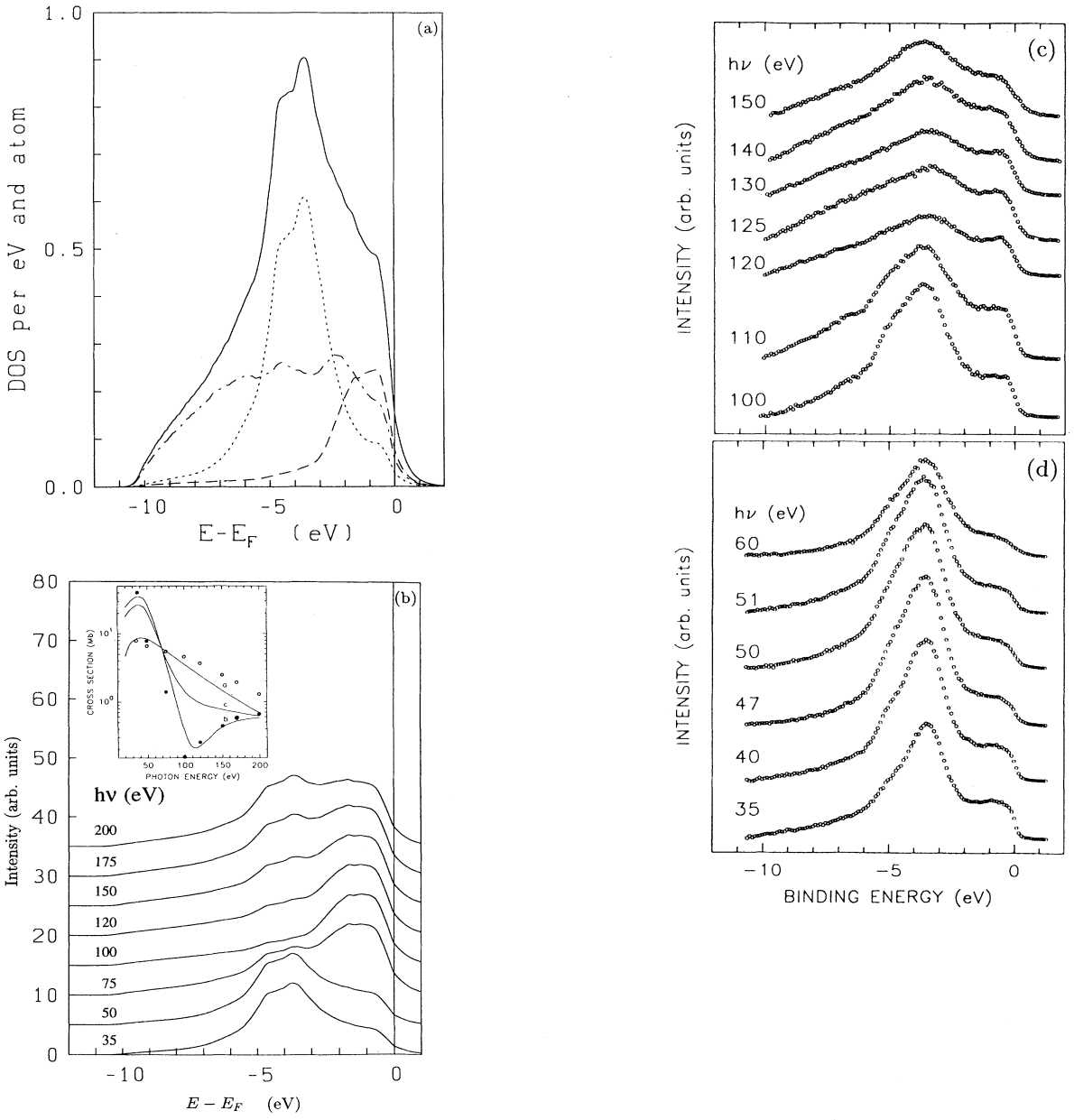

FIG. 24. (a) Total electronic DOS of i–Al-Pd-Mn, folded with a Fermi function and a Gaussian of width $\sigma = 0.3$ eV to account for the limited instrumental resolution. The dot-dashed, dotted, and dashed lines represent the contributions of the Al, Pd, and Mn atoms, respectively. (b) Calculated photoemission intensities for photon energies between 35 and 200 eV, using the partial photoionization cross sections shown in the inset [full lines — atomic cross section after Yeh and Lindau (Ref. 69), (a — Mn, b — Pd, c — concentration average of the partial Mn and Pd cross sections); full and empty circles — Pd and Mn cross sections calculated for the Al-Pd-Mn alloy, see text]. (c,d) Measured photoelectron spectra in the energy ranges of the Mn resonance and of the Cooper minimum in the Pd cross section. After Ref. 37.

B. Photoelectron spectroscopy

The total electronic DOS of the 8/5 approximant, folded with a Fermi function, is in reasonable agreement with the measured photoemission intensity for excitation energies in the ultraviolet range ($\hbar\omega \sim 40$ eV), see Fig. 24(a). However, in the experimental spectrum, the assignment of the local maxima near 0.7 eV and 3.5 eV binding energy to the Mn- and Pd-d bands is only tentative. Zhang *et al.*[37] have attempted to assess this assignment by exploiting the variation of the partial photoionization cross sections with the energy of the exciting photon. In the range 35 eV $< \hbar\omega <$ 200 eV, this variation arises from two different effects: (a) the resonant photoemission effect (i.e., the enhancement of the ionization cross section as the excitation energy exceeds the threshold of an inner excitation)[67] and (b) the Cooper-minimum effect resulting from the presence of a node in the radial part of the $4d$ wave functions.[68] For i-Al-Pd-Mn, a resonance in the photoemission spectrum occurs near the threshold for the Mn $3p \rightarrow 3d$ transition at about 47 eV. It causes a reduction of the partial ionization cross section for Mn-d states and allows us to assign the intensity near 0.7 eV binding energy to the Mn-d band [see Fig. 24(c)]. A theoretical analysis of the resonance effect requires a many-body treatment that goes beyond the scope of the present work.

The Cooper-minimum effect appears already in the partial photoionization cross section calculated for the free atoms,[69] solid-state effects may be estimated by recalculating the cross sections from the self-consistent potentials in a single-scatterer-final-state approximation as described by Redinger *et al.*[70,71] The basic assumptions are (a) dipole approximation to the electromagnetic field, (b) final states described as low energy electron diffraction states, and (c) neglect of wave vector conservation. For crystals, the last approximation is justified only for relatively high excitation energies, but for amorphous and quasicrystalline systems it can be extended to low photon energies.[61] Evidence for the relaxation of momentum conservation has also been claimed on the basis of the investigation of the optical properties.[72] The inset in Fig. 24(b) shows that the Cooper-minimum effect is much more pronounced than the Mn $3p \rightarrow 3d$ resonance effect, but solid-state effects are rather weak: the variation of the partial Pd and Mn cross section in the Al-Pd-Mn alloys with the excitation energy is essentially the same as in the free atom. Near $\hbar\omega \sim 100 - 150$ eV, the Pd cross section is reduced by nearly two orders of magnitude compared to $\hbar\omega \sim 30 - 50$ eV. One should also note that the single-scatterer-final-state approximation leads to a relatively high partial Mn cross section compared to the atomic limit. Fig. 24(b) shows the strong variation of the calculated photoemission intensity in this energy range. Compared to the experimentally measured intensities [see Fig. 24(c)], the calculated Cooper-minimum effect is even more pronounced, due to the sharp minimum in the Pd and the overestimate of the Mn cross section. This is not really disappointing, since the approximations underlying the calculation of the cross sections are fully justified only for higher photon energies. The important point is that the comparison of theory and experiment confirms the interpretation of the DOS features at 0.8 eV and 3.8 eV binding energy as arising from the Mn-d and P-d bands.

The essential question of the depth of the pseudogap at E_F is not resolved by the photoemission spectra available at the moment: this would require an energy resolution of the order of a few 0.01 eV. Such a resolution would also exceed that of our present recursion calculations. However, even if such a resolution could be achieved, we are not yet sure whether it would allow us to answer the question as to the internal structure of the pseudogap close to E_F: Is it legitimate to discuss the pseudogap effect in terms of a single gap induced by a dominant "quasi-BZ boundary" or does the gap consist in the quasiperiodic limit in reality of a hierachical structure of many very narrow gaps induced by the densely spaced "quasi-Γ points?" This question is intimately connected with the problem of the character of the eigenstates close to the Fermi level and we can make at least an attempt to answer that question by analyzing the TB eigenvectors for the low-order approximants.

VII. LOCALIZED AND EXTENDED EIGENSTATES OF ELECTRONS

The anomalous electronic transport properties of the stable icosahedral phases[14,15,32,33] cannot be explained by the existence of a pseudogap at the Fermi level alone: Their semi-insulating behavior is incompatible even with the lowest estimates for the DOS at E_F; it requires in addition a very low mobility of the conduction electrons. This raises the question of the character of the electronic eigenstates: extended as in crystals, or localized as in strongly disordered materials? The broken translational symmetry and the unusual transport properties suggest localization. On the other hand, the self-similarity of the quasicrystals as expressed by Conways theorem[73] (any local unit with diameter d is repeated within a distance $2d$) would cause an interaction of localized states through the overlapping exponential tails of the wave functions. For one-dimensional quasicrystals, it has been shown by renormalization-group techniques that the spectrum of a quasiperiodic chain is a Cantor set and that the eigenstates are critical, i.e., neither extended nor localized, with a power-law decay of the amplitudes.[74] For two-dimensional quasicrystals, numerical studies of simple tight-binding models suggest a similar behavior.[75] For rational approximants to realistic three-dimensional quasicrystals, numerical studies of the localization of vibrational eigenstates have been performed by two of the present authors.[76,77] It has been shown that localized (or rather confined, since they are repeated on the quasilattice according to Conways theorem) eigenstates with a characteristic topological support exist at certain characteristic energies coincident with the energies of stationary vibrational eigenstates and that the number of such confined states shows the expected τ^3 scaling with increasing order of the approximant. The character of the eigenstates is described by the participation ratio $P(E_n)$

given in terms of the eigenvectors of the Hamiltonian $\vec{e}_i(E_n)$ to the eigenvalue E_n, determining the amplitude of the wave function ψ_n at the site $\vec{R}_i$ by

$$P(E_n) = \frac{(\sum_i \sum_\alpha | e_{i\alpha}(E_n) |^2)^2}{N \sum_i (\sum_\alpha | e_{i\alpha}(E_n) |^2)^2} \quad . \tag{1}$$

$P(E_n) \sim O(1)$ describes extended states, $P(E_n) \sim O(1/N)$ localized states.

A calculation of the participation ratio for the electronic eigenstates requires the diagonalization of the TB Hamiltonian. For the states at the Γ point, this can be achieved for the 1/1 and 2/1 approximants — for the higher order approximants, even the block-diagonalized matrices would be too large. Figure 25(a) shows the participation ratios for the two versions of the 1/1 and 2/1 approximants (see Table I). The results show that most states are extended, but distinct minima in the participation ratio are found close to the peaks of the Pd- and Mn-d bands, i.e., also close to the Fermi surface. Figure 25(b) shows the distribution of the amplitudes of one of these more localized states [marked by the arrow in the lowest panel of Fig. 25(a)] in the cell of the 2/1-$M2$ approximant, projected on the (x, y) plane. One finds that the largest part of the intensity is indeed concentrated at four Mn sites situated at large distances from each other. These four Mn sites are just the four equivalent Mn sites in the 2/1 approximant generated by projecting the Mn atoms with the shortest distance from the center of the Mn acceptance domain at the n_1 node. The correlation between localization and the crystallographic description of the structure in the 6D space is further corroborated by plotting the inverse of the local amplitudes $\psi_{n,i}$ at the sites $\vec{R}_i$ of the eigenstates ψ_n against the length $| \vec{R}_\perp |$ of the corresponding vector in perpendicular space (Fig. 26). In general, we find that sites with a short $| \vec{R}_\perp |$ tend to support localized states, but states with a larger $| \vec{R}_\perp |$ can support extended as well as localized states. For the localized Mn states close to the Fermi level, however, we find that the correlation between a large amplitude $\psi_{n,i}$ and the distance $| \vec{R}_\perp |$ of the site $\vec{R}_i$ from the center of the acceptance domain is unique [see Fig. 26(b)]. No corresponding correlation holds for the localized Pd states at lower binding energy. Atoms projected from the center of the acceptance domain occupy sites with the full point-group symmetry of the node on which the atomic surface is centered — a large distance from this center leads to a lower point-group symmetry of the site (cf. also our discussion of the atomic-shell structure in Sec. II C). Thus, there is a correlation between local icosahedral order and localization.

There is also an interesting correlation between localization and the dispersion relations derived in Sec. V B from the Bloch spectral functions. In general, one would expect localized states to show very little dispersion. Comparing the diagram with the participation ratios [Fig. 25(a)] with the dispersion relations shown in Fig. 19, we find that the most localized (mostly Mn-based) states in the energy range from −1 eV to +1 eV correspond to stationary states, whose intensities are largest close to the "quasi-Brillouin-zone" boundaries.

States that are as strongly localized as that shown in Fig. 25(b) will make only a very small contribution to the electronic conductivity. This result shows that the low

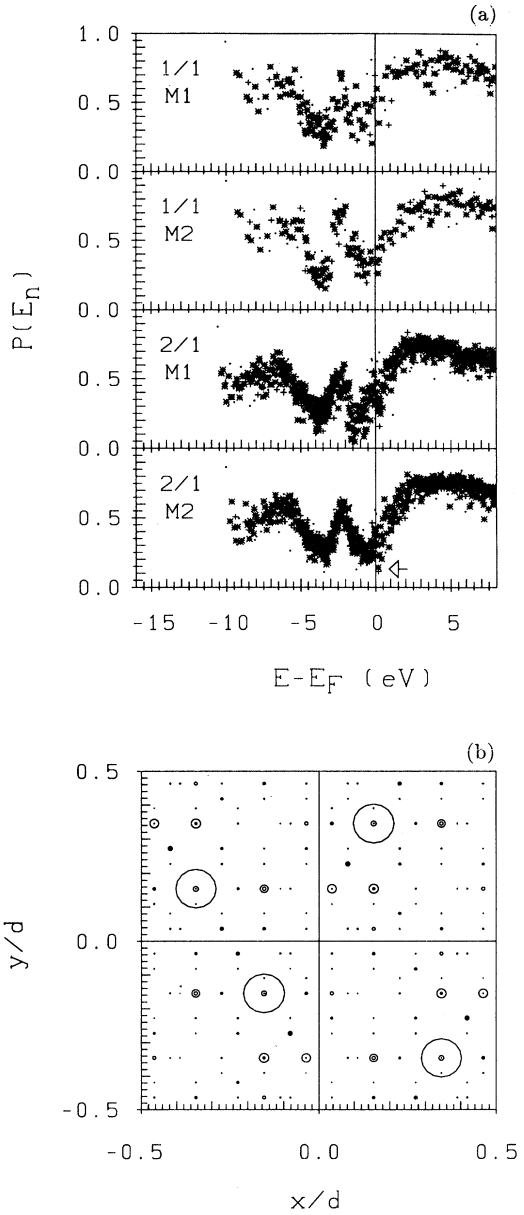

FIG. 25. (a) Participation ratios $P(E_n)$ of the electronic eigenstates for the two versions of the 1/1 and 2/1 approximants to i–Al-Pd-Mn with different chemical compositions. Different symbols refer to states transforming according to different irreducible representations. Part (b) shows the spatial distribution of the amplitudes of one of the more localized states very close to the Fermi level [marked by the arrow in the lowest panel of part (a)], projected on the (x, y) plane. The size of the symbols scales with the local amplitude. The four sites on which the amplitude is concentrated are the four equivalent Mn sites projected from the site closest to the center of the acceptance domain at the node n_1. See text.

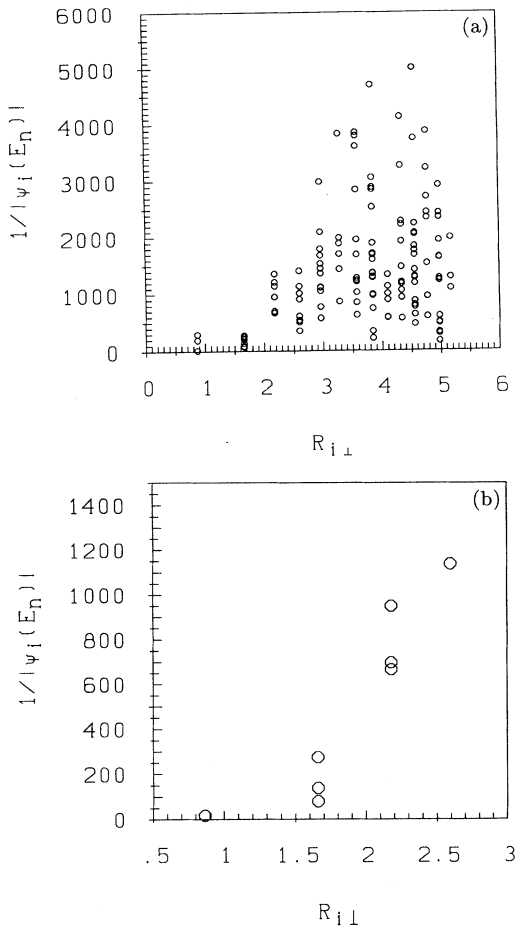

FIG. 26. Correlation between the local amplitude $\psi_{n,i}$ of the eigenstates ψ_n at the sites $\vec{R}_i$, plotted against the vector $\vec{R}_\perp$ in perpendicular space corresponding to that site. (a) All atomic sites, (b) Mn sites from the atomic surface at node n_1 only.

conductivity of the stable quasicrystals arises from both a low effective number of carriers and a low mobility of the states close to the Fermi energy. It also demonstrates that the hybridization of the conduction-band states with the Mn-d states is an important factor leading to these anomalous transport properties.

VIII. SUMMARY AND CONCLUSIONS

The aim of this paper is to achieve a thorough understanding of the electronic structure of icosahedral Al-Pd-Mn alloys in relation to the quasiperiodic atomic structure, of its role in determining the exceptional stability of the icosahedral phase and in the outstanding electronic transport properties.

A. Atomic structure

The first step in such a study has to be the construction of a model for the atomic structure. We have shown that the 6D-cut-and-projection model with the complex triacontahedral atomic surfaces proposed by Katz and Gratias[30] and Cockayne *et al.*[31] reproduces the available diffraction data reasonably well, except for effects associated with phason fluctuations whose effect on the electronic structure cannot be considered with today's computational tools. As a basis for the electronic-structure work, we have also constructed a series of rational approximants. There is an important lesson to be drawn from that exercise: It turns out that for the lowest-order approximants, it is not possible to find a model that reproduces at the same time the local atomic topology and the chemical order of the icosahedral phase. We have also analyzed in detail the atomic shell structure of the model and found that the surprisingly low coordination numbers inferred from the EXAFS data correlate with the low symmetry of certain sites.

B. Extended electronic eigenstates

The extended electronic eigenstates (total, local, and angular-momentum decomposed DOS and Bloch-spectral functions) have been studied for a hierarchy of approximants, using a variety of computational tools best adapted to the task. The most important results may be summarized as follows.

(a) A structure-induced pseudogap not too far from the Fermi level exists in all approximants with a local atomic topology close to that of the icosahedral phase. If the local atomic order is disturbed, the pseudogap is less pronounced. In the lowest-order approximants with the correct local topology (but the wrong chemical composition), the pseudogap is situated about 0.6 eV above E_F, a filling of the valence band up to the pseudogap corresponds exactly to the electron-per-atom ratio of the icosahedral phase. In the hierarchy of the approximants, the chemical composition changes in such a way that the position of the Fermi-level converges to that of the pseudogap. This is the first time that a systematic trend in the electronic structure of the approximants has been found. The consequence of this trend is that the Hume-Rothery-like mechanism for the stability works for the quasicrystal, but not for the lowest-order approximants. This explains why — in contrast to many other quasicrystal-forming alloys — 1/1-approximant phases have not been found in Al-Pd-Mn and related stable quasiperiodic alloys.

(b) The origin of the structure-induced pseudogap may again be traced back to the "quasi-Brillouin-zone" structure of reciprocal space:[10] The most intense "Γ points" are the origin of strong free-electron-like states [characterized by intense peaks in the Bloch spectral function $f(\vec{k}, E)$ following a parabolic dispersion law] that are degenerate at the "quasi-Brillouin-zone boundaries" (marked by the most intense special points). The interaction with the quasilattice lifts the degeneracy and leads to the formation of the pseudogap and stationary dispersion relations in the vicinity of these points. The transition-metal states show only weak dispersion, the formation of the characteristic s-d hybridization gap at the upper edge

of the d band enhances the "quasi-Brillouin-zone" effect. The existence of stationary states close to the Fermi energy is also of interest in connection with the possibility of having localized states influencing the electronic transport properties.

(c) The origin of the pseudogap has also been discussed in terms of the atomic shell structure of the quasicrystal. The results agree with the conclusions drawn from the "quasi-Brillouin-zone" picture: the pseudogap is most pronounced in the local DOS on the highly symmetric Al shells surrounding a central atom; the depth and width of the pseudogap on a certain shell depends to some degree on the occupancy of the neighboring shells: the hybridization of the Al-s,p states with the transition-metal (especially Mn)-d states tends to widen the pseudogap.

(d) The calculated band structure is in good agreement with the existing photoemission and soft-x-ray emission and absorption spectra. This concerns, in particular, the widths and positions of the Al, Pd, and Mn subbands and the existence of the pseudogap at E_F. However, due to limited resolution, spectroscopy cannot give a quantitative assessment of the DOS at E_F. We also have to admit that the TB-LMTO real-space recursion approach to the electronic structure of the largest approximants has a limited resolution: it is possible that the very low DOS at E_F deduced from the electronic-specific-heat experiment[34,35] refer to the DOS in a pseudogap that is much narrower than the resolution of the TB-LMTO calculation.

C. Localized electronic eigenstates

For the 1/1 and 2/1 approximants, we have exploited the possibility of studying the localization properties of the electronic eigenstates as characterized by the participation ratios (determined by the TB eigenvectors of each state). The results show that most eigenstates are extended, but we find low participation ratios at the energies close to the maxima in the Pd- and Mn-d-band DOS (for the Mn band this is very close to E_F). Analyzing the spatial distribution of the amplitudes of the more localized states leads to a very interesting correlation between localization and symmetry: The localized states closest to the Fermi energy are concentrated on the Mn sites closest to the center of the Mn-acceptance domain in perpendicular space, i.e., with the highest degree of icosahedral symmetry. These states are also correlated to stationary points in the dispersion relations close to the "quasi-Brillouin-zone" boundaries. The tendency for states close to the Fermi energy to be localized is important for the understanding of the "semimetallic" transport properties of the stable quasicrystals. However, the correlation between icosahedral symmetry and localization needs to be further investigated.

ACKNOWLEDGMENT

This work has been supported by the Austrian Science Foundation under Contract No. P9678-PHYS.

* Permanent address: Institute of Physics, Slovak Academy of Sciences, SK 84228 Bratislava, Slovakia.

[1] D. Shechtmann, I. Blech, D. Gratias, and J. W. Cahn, Phys. Rev. Lett. **53**, 1951 (1984).
[2] For recent reviews see, e.g., *Quasicrystals — The State of the Art,* edited by D.P. DiVincenzo and P. J. Steinhardt (World Scientific, Singapore, 1991); *Quasicrystals,* edited by T. Fujiwara and T. Ogawa (Springer, Berlin, 1990); C. Janot, *Quasicrystals — A Primer* (Oxford University Press, Oxford, 1992).
[3] S. J. Poon, Adv. Phys. **41**, 303 (1992).
[4] U. Mizutani, in *Materials Science and Technology,* edited by R. W. Cahn and P. Haasen (Verlag Chemie, Weinheim, 1993), Vol. 3.
[5] D. A. Bancel and P. A. Heiney, Phys. Rev. B **33**, 7917 (1986).
[6] A. P. Smith and N. W. Ashcroft, Phys. Rev. Lett. **59**, 1356 (1987).
[7] J. Friedel and F. Denoyer, C. R. Acad. Sci. (Paris) **305**, 171 (1987).
[8] T. Fujiwara and T. Yokokawa, Phys. Rev. Lett. **66**, 333 (1991).
[9] T. Fujiwara, J. Non-Cryst. Solids **156-158**, 865 (1993).
[10] J. Hafner and M. Krajčí, Phys. Rev. Lett. **68**, 2321 (1992); Phys. Rev. B **47**, 11 795 (1993).
[11] M. Windisch, M. Krajčí, and J. Hafner, J. Phys. Condens. Matter **6**, 6977 (1994).
[12] A. P. Tsai, A. Inoue, and T. Masumoto, Jpn. J. Appl. Phys. **26**, L1505 (1987); **27**, L1587 (1988).
[13] A. P. Tsai, A. Inoue, and T. Masumoto, Sci. Rep. Res. Inst. Tohoku Univ. Ser. A **36**, 99 (1991).
[14] F. S. Pierce and S. J. Poon, Science **261**, 737 (1993).
[15] T. Klein, C. Berger, D. Mayou, and F. Cyrot-Lackmann, Phys. Rev. Lett. **66**, 2971 (1991).
[16] M. de Boissieu, P. Stephens, M. Boudard, C. Janot, D. L. Chapman, and M. Audier, Phys. Rev. Lett. **72**, 3538 (1994), and references cited therein.
[17] M. Krajčí and J. Hafner, Europhys. Lett. **27**, 147 (1994).
[18] F. Hippert, L. Kandel, Y. Calvayrac, and B. Dubost, Phys. Rev. Lett. **69**, 2086 (1992).
[19] A. P. Tsai, A. Inoue, Y. Yokoyama, and T. Masumoto, Philos. Mag. Lett. **61**, 9 (1990); Jpn. J. Appl. Phys. **29**, L 1161 (1990).
[20] A. P. Tsai, A. Inoue, and T. Masumoto, Philos. Mag. Lett. **62**, 95 (1990).
[21] C. Janot, J. Pannetier, J. M. Dubois, and M. de Boissieu, Phys. Rev. Lett. **62**, 450 (1989).
[22] M. Boudard, M. de Boissieu, C. Janot, J. M. Dubois, and C. Dong, Philos. Mag. Lett. **64**, 197 (1991).
[23] A. P. Tsai, H. S. Chen, A. Inoue, and T. Masumoto, Phys. Rev. B **43**, 8782 (1991).
[24] M. Boudard, M. de Boissieu, C. Janot, G. Heger, C. Beeli, H. U. Nissen, H. Vincent, R. Ibberson, M. Audier, and J. M. Dubois, J. Phys. Condens. Matter **4**, 10 149 (1992).
[25] S. W. Kycia, A. I. Goldman, T. A. Lograsso, D. W. Delaney, M. Sutton, E. Dufresne, R. Brüning, and B. Rodricks, Phys. Rev. B **48**, 3544 (1993).
[26] M. de Boissieu, P. Stephens, M. Boudard, and C. Janot, J. Phys. Condens. Matter **6**, 363 (1994).
[27] A. Sadoc and J. M. Dubois, J. Non-Cryst. Solids **153-154**, 83 (1993).
[28] M. Audier, M. Durand-Charre, and M. de Boissieu, Philos.

Mag. B **68**, 607 (1993), and further references cited therein.
[29] M. Cornier-Quinandon, A. Qivy, S. Lefebvre, E. Elkaim, G. Heger, A. Katz, and D. Gratias, Phys. Rev. B **44**, 2071 (1991).
[30] A. Katz and D. Gratias, J. Non-Cryst. Solids **153-54**, 187 (1993).
[31] E. Cockayne, R. Phillips, X. B. Kan, S. C. Moss, J. L. Robertson, T. Ishimasa, and M. Mori, J. Non-Cryst. Solids **153-154**, 140 (1993).
[32] P. Lanco, T. Klein, C. Berger, F. Cyrot-Lackmann, G. Fourcadot, and A. Sulpice, Europhys. Lett. **18**, 227 (1992).
[33] S. Takeuchi, H. Akiyama, N. Naito, T. Shibuya, T. Hashimoto, K. Edagawa, and K. Kimura, J. Non-Cryst. Solids **153-154**, 353 (1993).
[34] M. A. Chernikov, A. Bernasconi, C. Beeli, A. Schilling, and H. R. Ott, Phys. Rev. B **48**, 3058 (1993).
[35] M. A. Chernikov, A. Bernasconi, C. Beeli, and H. R. Ott, Europhys. Lett. **21**, 767 (1993).
[36] Z. M. Stadnik and G. Stroink, Phys. Rev. B **47**, 100 (1993).
[37] G. W. Zhang, Z. M. Stadnik, A. P. Tsai, and A. Inoue, Phys. Lett. A **186**, 345 (1994); Phys. Rev. B **50**, 6696 (1994).
[38] E. Belin, Z. Dankhazi, A. Sadoc, and J. M. Dubois, J. Phys. Condens. Matter **6**, 8771 (1994).
[39] G. W. Zhang, Z. M. Stadnik, A. P. Tsai, A. Inoue, and T. Miyazaki (unpublished).
[40] A. Waseda, H. Morioka, K. Kimura, and H. Ino, Philos. Mag. Lett. **65**, 25 (1992).
[41] O. K. Andersen, Phys. Rev. B **12**, 3060 (1975); H. L. Skriver, *The LMTO Method* (Springer, Berlin 1984).
[42] G. Kresse and J. Hafner, Phys. Rev. B **47**, 558 (1993); **48**, 13 115 (1993).
[43] G. Kresse and J. Hafner, Phys. Rev. B **49**, 14 251 (1994).
[44] O. K. Andersen and O. Jepsen, Phys. Rev. Lett. **53**, 2571 (1984); O. K. Andersen, D. Jepsen, and M. Šob, in *Electronic Band Structure and its Applications,* edited by M. Youssouff (Springer, Berlin 1987).
[45] S. K. Bose, S. S. Jaswal, O. K. Andersen, and J. Hafner, Phys. Rev. B **37**, 9955 (1988).
[46] M. de Boissieu, P. Stephens, M. Boudard, C. Janot, D. L. Chapman, and M. Audier, J. Phys. Condens. Matter **6**, 10 725 (1994).
[47] J. W. Cahn, D. Shechtman, and D. Gratias, J. Mater. Res. **1**, 13 (1986).
[48] A. Sadoc and J. M. Dubois, Philos. Mag. B **66**, 541 (1992).
[49] M. Windisch, Thesis, Technische Universität Wien, 1995.
[50] K. Niizeki, J. Phys. A **22**, 4295 (1989).
[51] K. Niizeki and T. Akamatsu, J. Phys. Condens. Matter **2**, 2759 (1989).
[52] M. C. Payne, M. P. Teter, D. C. Allan, T. A. Arias, and J. D. Joannopoulos, Rev. Mod. Phys. **64**, 1045 (1992).
[53] G. Kresse and J. Hafner, J. Phys. Condens. Matter **6**, 8265 (1994).
[54] A. M. Rappe, K. M. Rabe, E. Kaxiras, and J. D. Joannopoulos, Phys. Rev. B **41**, 1227 (1990).
[55] D. Vanderbilt, Phys. Rev. B **41**, 7892 (1990).
[56] W. H. Press, B. P. Flannery, S. A. Teukolsky, and W. T. Vetterling, *Numerical Recipes: The Art of Scientific Computing* (Cambridge University Press, Cambridge, 1986).
[57] O. Jepsen and O. K. Andersen, Solid State Commun. **9**, 1762 (1971).
[58] G. Trambly de Laissardière and T. Fujiwara, Phys. Rev. B **50**, 5999 (1994).
[59] T. Fujiwara, Phys. Rev. B **40**, 942 (1989).
[60] P. Oelhafen, in *Glassy Metals II,* edited by H. Beck and H. J. Güntherodt (Springer, Berlin 1983), p. 283.
[61] W. Jank, C. Hausleitner, and J. Hafner, Europhys. Lett. **16**, 473 (1991).
[62] C. Hausleitner, M. Tegze, and J. Hafner, J. Phys. Condens. Matter **4**, 9557 (1992).
[63] G. V. Raynor, Prog. Met. Phys. **1**, 531 (1949).
[64] V. Heine, D. Bullett, R. Haydock, and M. J. Kelly, in *Solid State Physics: Advances in Research and Applications,* edited by H. Ehrenreich, D. Turnbull, and F. Seitz (Academic Press, New York, 1980), Vol. 35.
[65] C. M. M. Nex, J. Phys. A **11**, 653 (1978).
[66] M. U. Lucchini and C. M. M. Nex, J. Phys. C **20**, 3125 (1987).
[67] L. C. Davis, J. Appl. Phys. **59**, R25 (1986).
[68] G. Rossi, I. Lindau, L. Braicovich, and I. Abbati, Phys. Rev. B **28**, 3031 (1983).
[69] J. J. Yeh and I. Lindau, At. Data Nucl. Data Tables **32**, 1 (1985).
[70] S. Redinger, P. Marksteiner, and P. Weinberger, Z. Phys. B **63**, 321 (1986).
[71] W. Jank and J. Hafner, J. Phys. Condens. Matter **2**, 5065 (1990); Phys. Rev. B **45**, 2739 (1992).
[72] D. N. Basov, F. S. Pierce, P. Volkov, S. J. Poon, and T. Timusk, Phys. Rev. Lett. **73**, 1865 (1994).
[73] M. Gardner, Sci. Am. **236**, 110 (1977).
[74] M. Kohomoto and B. Sutherland, Phys. Rev. B **34**, 3849 (1986).
[75] H. Tsunetsugu, T. Fujiwara, K. Ueda, and T. Tokihiro, Phys. Rev. B **43**, 8879 (1991).
[76] J. Hafner and M. Krajčí, Phys. Rev. B **47**, 1084 (1993); J. Phys. Condens. Matter **5**, 2489 (1993).
[77] M. Krajčí and J. Hafner (unpublished).
[78] W. Jank and J. Hafner, J. Phys. Condens. Matter **2**, 5065 (1990); Phys. Rev. B **45**, 2739 (1992).

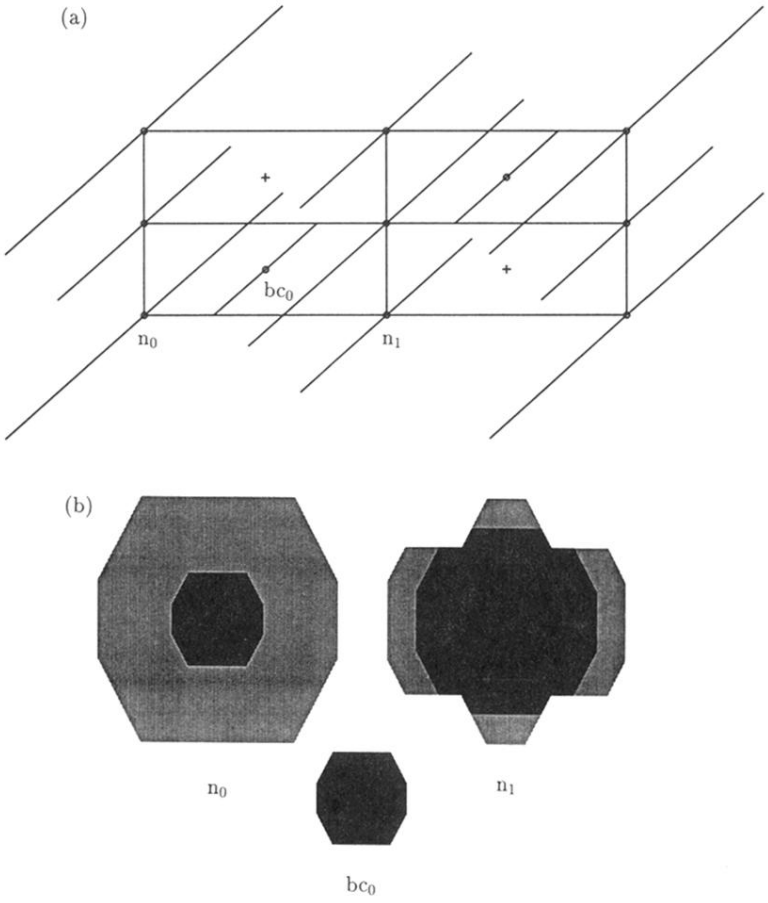

FIG. 1. Illustration of our model for the structure of icosahedral Al-Pd-Mn. (a) Section through the 6D space containing the fivefold axes in $E_{\parallel}$ and $E_{\perp}$. Atomic surfaces are placed at the nodes n_i and the body centers bc_0 of a hypercubic lattice. Since the atomic surfaces placed on the even and odd nodes (n_0 and n_1) are not equivalent, the symmetry of the 6D lattice is face-centered cubic. (b) Cross sections through the atomic surfaces (calculated for a 13/8 approximant). The Mn cores at the n_0 and n_1 nodes are represented by the darkest shading; the lighter shading represents the outer Pd and Al shells at these nodes and the Pd surface at the bc_0 position.

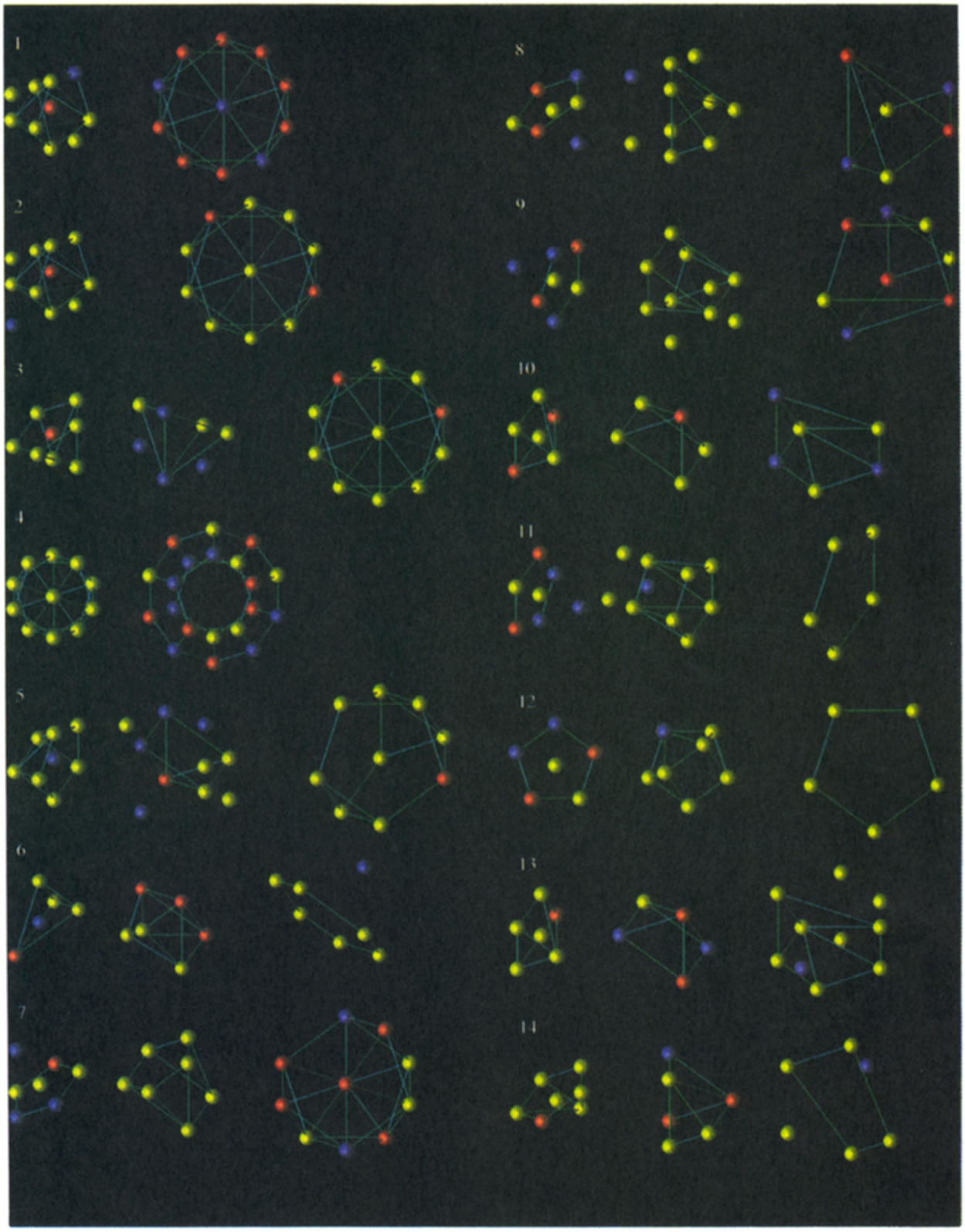

FIG. 7. Coordination shells for the 14 crystallographically inequivalent sites in the 1/1 approximant to *i*-Al-Pd-Mn. Yellow — Al atoms; blue — Pd atoms; red — Mn atoms. The green lines connect the vertices in each shell with exactly the same distance from the central atoms; atoms not connected by green lines are situated at a slightly different distance. Cf. text.

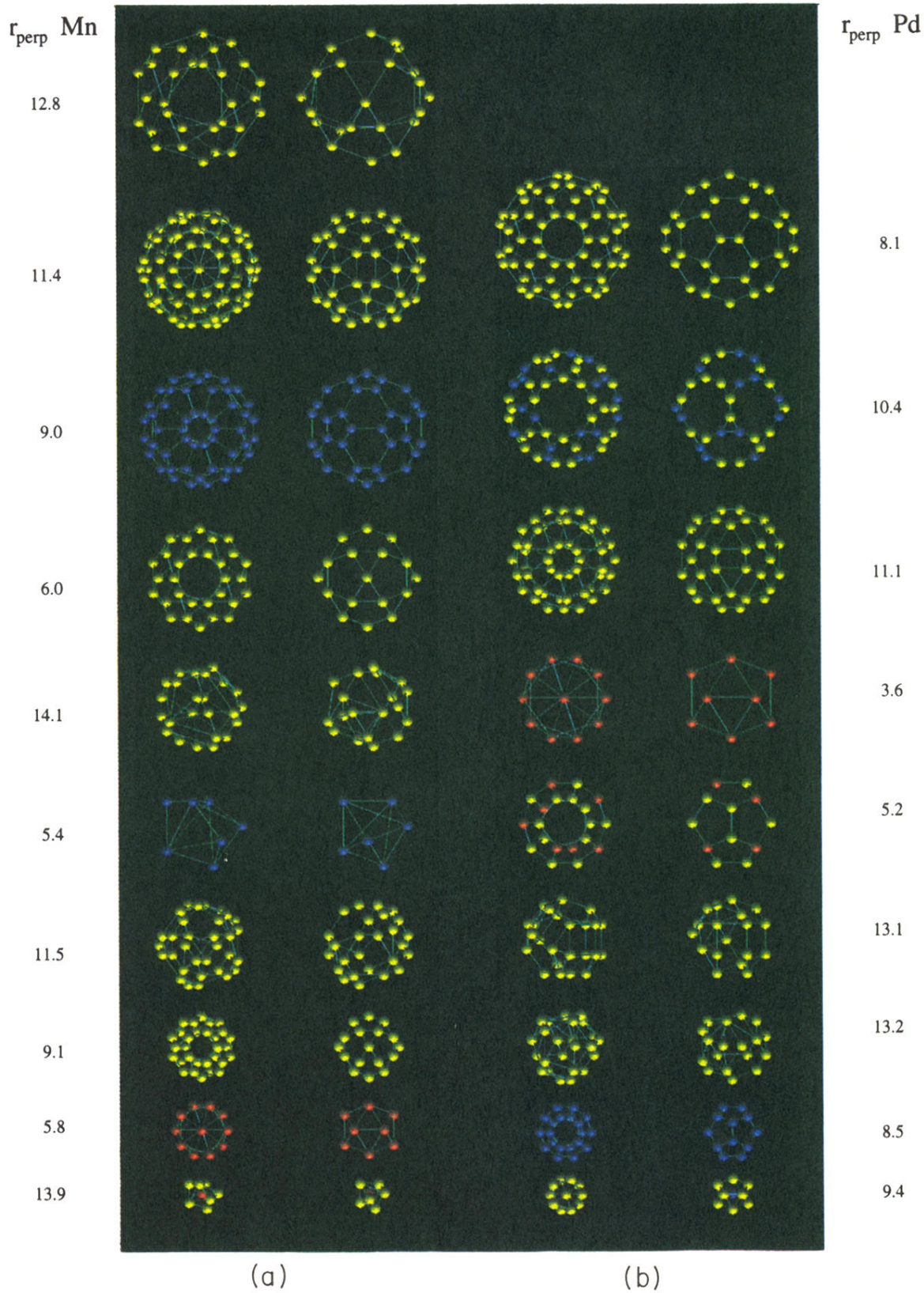

FIG. 8. (a) Coordination shells around a sevenfold Mn site in the 5/3 approximant to *i*-Al-Pd-Mn. The numbers listed give the number of the coordination shell and the radius of the corresponding shell in $E_\perp$ (in units of the lattice constant of the cubic lattice in $E_\perp$). The colors have the same meaning as in Fig. 7. See text. (b) Coordination shells around the bc_0 (twelvefold) Pd site in the 5/3 approximant to *i*-Al-Pd-Mn. For explanation of symbols, see Figs. 7 and 8(a).